



Dual effect of Se(IV) and bentonite microbial community interactions on the corrosion of copper and Se speciation: Implication on repository safety assessment

Marcos F. Martinez-Moreno^{a,*}, Cristina Povedano-Priego^a, Mar Morales-Hidalgo^a, Adam D. Mumford^b, Guillermo Lazuen-Lopez^a, Elisabet Aranda^c, Ramiro Vilchez-Vargas^d, Pier L. Solari^e, Yon Ju-Nam^b, Fadwa Jroundi^a, Jesus J. Ojeda^b, Mohamed L. Merroun^a

^a Faculty of Sciences, Department of Microbiology, University of Granada, Granada, Spain

^b Department of Chemical Engineering, Faculty of Science and Engineering, Swansea University, Swansea, United Kingdom

^c Institute of Water Research, Department of Microbiology, University of Granada, Granada, Spain

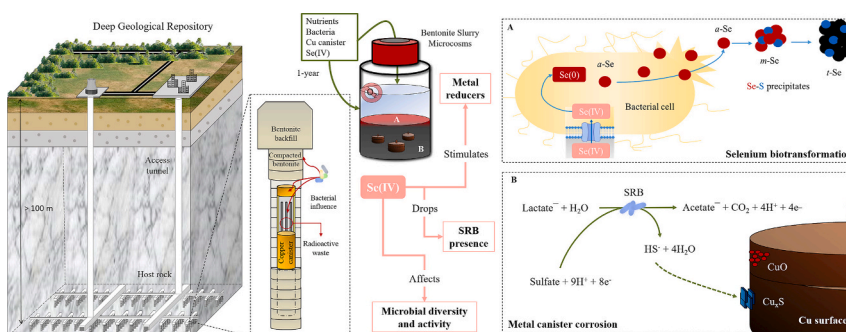
^d Medical Department II, University Hospital, Ludwig-Maximilians-Universität, Munich, Germany

^e MARS Beamline, Synchrotron SOLEIL, L' Orme des Merisiers, Départementale 128, Saint-Aubin, France

HIGHLIGHTS

- Se(IV) and bentonite tyndallization delay microbial-influenced geochemical processes.
- Bacterial consortium and nutrients addition accelerate microbial activity.
- Se(IV) reduces the abundance of some SRB while stimulate Se-tolerant genera.
- Bentonite-community Se-tolerant bacteria reduce Se(IV) to α -Se(0) nanospheres.
- Sulfide produced by SRB activity result in the formation of Cu_2S on Cu-surface.

GRAPHICAL ABSTRACT



ARTICLE INFO

Editor: Frederic Coulon

Keywords:

Deep geological repository
Selenium speciation
Bentonite
Bacteria
Copper biocorrosion

ABSTRACT

The Deep Geological Repository (DGR) design, the internationally safest option for the long-term disposal of high-level radioactive waste (HLW), features metal canisters encased in compacted bentonite clay and embedded deep within a host rock. Despite presenting a hostile environment for microorganisms, DGRs scenarios with favorable microbial-activity conditions must be considered for the safety assessment of this disposal. This study investigated the impact of Se(IV), as a natural analogue of ^{79}Se present in the HLW, in anoxic microcosms of bentonite slurry spiked with a bacterial consortium and amended with lactate, acetate, and sulfate as electron donors/acceptor. The addition of the bacterial consortium promoted the rate of Se(IV) reduction to Se(0), while the tyndallization (heat-shock) of bentonite slowed this process. Se(IV) reduced the relative abundance of most genera of sulfate-reducing bacteria (SRB), while stimulating the abundance of Se-tolerant bacteria, which played an important role in Se(IV) reduction. Moreover, it was observed that lactate was the preferred electron donor,

* Corresponding author.

E-mail address: mmartinezm@ugr.es (M.F. Martinez-Moreno).

<https://doi.org/10.1016/j.scitotenv.2025.178613>

Received 16 November 2024; Received in revised form 3 January 2025; Accepted 20 January 2025

Available online 30 January 2025

0048-9697/© 2025 The Authors. Published by Elsevier B.V. This is an open access article under the CC BY license (<http://creativecommons.org/licenses/by/4.0/>).

linking to the production and subsequent consumption of acetate. X-ray absorption spectroscopy (XAS) and high-resolution transmission electron microscopy (HRTEM) revealed the reduction of Se(IV) forming amorphous Se(0) nanospheres. In addition, HRTEM showed that the biogenic Se(0) undergo a biotransformation to more stable crystalline forms, contributing to the immobilization of Se in the case of HLW release. Additionally, the sulfide generated by the activity of SRB reacted with Cu producing corrosion products (Cu_2S) on the surface of the copper material.

1. Introduction

One of the challenges associated with the nuclear power industry is the final disposal of spent nuclear fuel, which is classified as high-level radioactive waste (HLW). Among the radionuclides generated by the fission of uranium fuel, selenium-79 (^{79}Se) stand out being considered a key mobile fission product of particular concern in the disposal of spent fuel and HLW (Hassan et al., 2021; Abdalla et al., 2020). Moreover, the chemical toxicity of Se depends on its oxidation state (Ruiz-Fresneda et al., 2020; Avendaño et al., 2016). At higher oxidation states (IV and VI), selenium is more soluble and thus mobile, and it is therefore considered toxic. At lower oxidation states (0 and -II), Se species are less soluble and mobile, exhibiting scarce environmental impact. The emission of beta particles during its radioactive decay and its half-life (3.77×10^5 years) makes ^{79}Se a key determinant of the long-term radiological impact of a deep geological repository (DGR) (Jörg et al., 2010; Bienvenu et al., 2007). Ionizing radiation emitted by the radioisotope ^{79}Se could contribute to the abiotic reduction of this metalloid in an aqueous environment. Le Caër (2011) reported that when a radiation beam crosses a system containing sodium selenite dissolved in water, it can promote the radiolysis of the water molecules, producing large amounts of reducing agents (e.g., hydrated electrons, hydrogen radicals, or hydroxyl radicals). These generated products exhibit a reduction potential that could reduce Se(IV) to Se(0), thereby facilitating the prevalence of higher selenium oxidation states (El-Batal et al., 2020). However, this study aimed to evaluate the role of microbial communities in bentonite to assess the potential selenium bioreduction as an additional barrier in the event of a waste leakage. Since ionizing radiation can affect various factors, including metal oxidation states, microbial viability and diversity, and the corrosion of metal canisters, this research builds on providing a baseline understanding of the processes occurring in the absence of radiation exposure.

The most widely accepted solution for the long-term confinement of the HLW is the DGR, whose main aim is to maintain its integrity for hundreds to millions of years, preventing the release of radionuclides into the environment, until their radiotoxicity decays to natural levels (WNA, 2024; Batandjieva et al., 2009). DGR's multi-barrier system design consists of corrosion-resistant metal canisters surrounded by a backfill and sealing material, and placed several hundred meters into a stable geological formation.

The material of DGR barriers depends on each country's approach. For example, Canada, Korea, Sweden, and Finland have proposed or implemented a copper coat for their metal canisters (Hall et al., 2021). Furthermore, the proposed material for buffering and sealing DGRs is compacted bentonite clay. This material offers mechanical support for canisters and helps to seal cracks. Compacted bentonite would prevent water infiltration from reaching the canisters, and hinder radionuclides diffusion (García-Romero et al., 2019). In Spain, the suggested clay material for the DGR is the bentonite from "El Cortijo de Archidona" (Almería), also known as FEBEX (Huertas et al., 2021; Villar et al., 2006). Due to the fact that bentonites are not sterile, the characterization of their microbial community structure and composition is crucial to assess the repository's long-term stability and safety (Meleshyn, 2011). While the conditions within the DGR may not be optimal for microbial growth, the permeation of nutrient-containing pore water from the host rock might promote the development and activity of microorganisms. The latter may cause microbially induced corrosion (MIC)

of the metal canisters, contribute to the production of a gaseous phase, alter inherent properties of the bentonite, and influence mobilization or immobilization of radionuclides (Ruiz-Fresneda et al., 2023).

After the repository sealing, an anoxic environment could prevail due to microbial activity and canister corrosion (Payer et al., 2019; Keech et al., 2014). Once this environment is established, anaerobic bacteria such as sulfate-reducing bacteria (SRB) and iron-reducing bacteria (IRB) might remain active negatively affecting the DGR barriers through processes such as MIC promotion, bentonite illitization, and sulfate reduction to sulfide (main canister corrosion agent) (Morales-Hidalgo et al., 2024; Pentráková et al., 2013; Liu et al., 2012; Shelobolina et al., 2003). The sulfide generated by SRB, will be favored in areas further from the canisters, where lower temperatures and greater water activity could prevail (Bengtsson and Pedersen, 2017). This biogenic sulfide may diffuse through the bentonite material and reach the canister surface causing corrosion and the release of HLW in the worst-case scenario.

Despite the compaction of bentonite into blocks within the DGR, which should inhibit microbial activity, all possible failure scenarios must be considered for safety assessments. Therefore, the present work simulated a "worst-case" scenario where a release of selenium could take place, and the bentonite turns to slurry form enriched with nutrients. To assess the impact of microorganisms' activity in the Spanish bentonite, optimal growth conditions were established by setting up bentonite slurry microcosms amended with electron donors (acetate and lactate) and acceptor (sulfate). Furthermore, the addition of 2 mM of Se(IV) acted as a natural analogue of ^{79}Se present in the HLW.

Hence, this study aimed to examine, using an interdisciplinary approach, the impact of Se(IV) amendment on the microbial communities of Spanish bentonite and the subsequent effect of these microorganisms on the geochemical evolution of the microcosms during one year of anoxic incubation. Additionally, an early-stage characterization of microbial-mediated selenium reduction products and copper corrosion was conducted. Our findings highlight the potential impact of bentonite microorganisms, thriving under nutrient influx from water filtration on the clay and long-term release of HLW from DGR.

2. Materials and methods

2.1. Sampling of bentonite clay

Bentonite was aseptically collected from "El Cortijo de Archidona" site (Spain), disaggregated, dried, and ground as specified in Martínez-Moreno et al. (2023). The chemical composition of the natural bentonite was previously published in Martínez-Moreno et al. (2024b) and detailed in Supplementary Table S1.

2.2. Anoxic microcosms' assembly: specifications, content, and sampling

Microcosms were set up following the procedure stated by Martínez-Moreno et al. (2024b) with some modifications. Briefly, 50 g of ground bentonite were deposited into sterilized borosilicate glass bottles. Since bentonite is difficult to completely sterilize by means of heat treatments (Martínez-Moreno et al., 2024a), one set of bentonite-containing bottles (StB samples) were tyndallized (autoclave 110 °C for 45 min, 3 consecutive days) in order to reduce the presence and activity of indigenous bentonite bacteria (hereafter known as heat-shocked

bentonites). To stimulate bacterial activity, some microcosms (electron donors/acceptor-containing microcosms -eD-) were added with a final concentration of 30 mM acetate, 10 mM lactate, and 20 mM sulfate. Bacterial consortium-containing microcosms (BC) were spiked with a BPAS consortium (Martinez-Moreno et al., 2024b), composed of four bacterial strains previously detected in the Spanish bentonite (*Bacillus* sp. BII-C3, *Pseudomonas putida*, *Amycolatopsis ruanii*, and *Stenotrophomonas bentonitica*), with an initial optical density (OD₆₀₀) of 0.4 each. Additionally, three sterilized high-purity oxygen free copper mini canisters (Cu-mCan) (Martinez-Moreno et al., 2024b) were deposited into each microcosm for corrosion studies.

All the microcosms were supplemented with a final concentration of 2 mM sodium selenite [Se(IV)] for the interaction studies. For this propose, 1 M of sodium selenite stock solution (Na₂SeO₃ • Sigma-Aldrich) was prepared and sterilized by 0.22 µm pore-sized filters.

Lastly, the final volume of the microcosms was calculated taking into account all the solutions added and were filled up to 230 mL with equilibrium water (EW) (elaboration procedure and chemical composition previously detailed in Martinez-Moreno et al., 2024b).

In summary, different treatments were considered (sample code between brackets): i) bentonite or heat-shocked bentonite (B – StB); ii) acetate, lactate, and sulfate addition (eD); and iii) spiked with the BPAS consortium (BC). Selenium-free treatments were previously published in Martinez-Moreno et al. (2024b). Overall, 24 microcosms were prepared (8 treatments in triplicate) and anoxically incubated at 28 °C for one year. Sample ID and the content of each treatment are summarized in Table 1.

The sampling procedure from the different microcosms for further analyses was carried out within an anaerobic chamber. The step-by-step process of the experimental setup and sampling is shown in Fig. 1.

2.3. Geochemical analyses

To determine the changes in physicochemical parameters, the supernatant (liquid phase) was collected from each microcosm within an anaerobic chamber. Samples were measured at 45, 90, 135, and 365 days of incubation, previously filtered through a 0.22 µm filter. pH measurements were performed by Advanced Digital Handheld Portable Meter HQ40D from Hach, previously calibrated with commercially available reference solutions (pH 4.00 and 7.00).

The percentage of acetate, lactate and sulfate from the amended treatments (eD) was measured by high pressure ion chromatography (HPIC) by a 925 Eco ICE Methrom Hispania (Herisau, Switzerland). Measurement specifications were followed in detail according to Martinez-Moreno et al. (2024b).

2.4. Microbial DNA extraction, sequencing, and bioinformatic analyses

Total DNA was extracted from the bentonite of the microcosms after

Table 1

Sample ID and content of the different microcosms. All microcosms contained each three Cu mini-canisters (Cu-mCan) and 2 mM of Se(IV). The microcosms were set up in triplicate and anoxically incubated at 28 °C. ALS: acetate, lactate and sulfate concentrations; BPAS: bacterial consortium; +: presence; -: absence.

Sample ID	Bentonite	ALS (mM)	BPAS	Se(IV)
B.eD.Se.BC	Non-heat-shocked	30:10:20	+	2 mM
B.Se.BC		–	+	
B.eD.Se		30:10:20	–	
B.Se		–	–	
StB.eD.Se.BC	Heat-shocked	30:10:20	+	
StB.Se.BC		–	+	
StB.eD.Se		30:10:20	–	
StB.Se		–	–	

Glossary: B: bentonite, StB: heat-shocked bentonite, eD: addition of electron donors/acceptor (ALS), Se: 2 mM of Se(IV), BC: spiked with BPAS consortium.

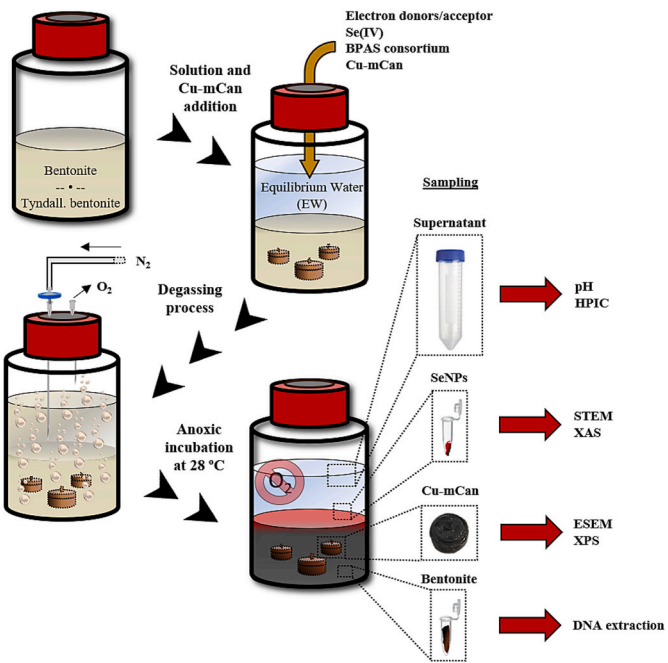


Fig. 1. Step-by-step of the anaerobic microcosm's assembly, specifications, content, and sampling.

45 days of incubation according to the protocol detailed by Povedano-Priego et al. (2021). The concentration of the obtained DNA was measured using the Qubit 3.0 Fluorometer (Life Technology, Invitrogen™).

For library preparation, the steps were followed as described in detail by Martinez-Moreno et al. (2024b). The obtained FastQ files were processed and normalized using R 4.2.1 software (R Core Team, 2022). The assignment of phylotypes to taxonomic affiliation was performed using a Bayesian classification (80 % pseudo-bootstrap threshold). Explicet 2.10.5 software (Robertson et al., 2013) was employed for the calculation of the relative abundance and alpha diversity indices. A matrix based on the Bray-Curtis algorithm through principal coordinate analysis (PCoA) was constructed to evaluate the similarity between samples at the genus level using Past4 software (Hammer and Harper, 2001). Additionally, a heatmap was generated to visualize the operational taxonomic units (OTUs) causing dissimilarity between samples.

2.5. Characterization of selenium reduction products (SeRPs)

2.5.1. Microscopic analyses

Samples from the interface bentonite:EW (Fig. 1) were recovered from the microcosms after 45 days of incubation and analyzed by ultra-high resolution transmission electron microscope and high-angle annular dark-field (HRTEM-HAADF) FEI TITAN G2. One mL of each homogenized interface was centrifugated at 10,000 g for 5 min and prepared as thin sections for microscopy analyses after contrasting with osmium for the visualization of the bacterial cells. Afterwards, selenium reduction products (SeRPs) were characterized by selected-area electron diffraction (SAED) and high-resolution transmission electron microscopy (HRTEM) combined with fast Fourier transform (FFT).

2.5.2. X-ray absorption spectroscopy (XAS) analysis

The interface from the microcosms were dried and powered for XAS analysis. The powders were spread and pressed onto Kapton tape (10 mm × 3 mm area) and sealed between additional layers. Selenium references, including sodium selenate [Se(VI)], sodium selenite [Se(IV)], and elemental selenium [Se(0)] foil, were prepared following the method described by Ruiz-Fresneda et al. (2020).

Se K-edge XAS data collected in fluorescence mode for the samples were obtained at the SOLEIL synchrotron's MARS beamline (France). This bending magnet beamline is dedicated to the multi-analyses of radioactive materials (Sitaud et al., 2012). Detailed information about XAS measurements is specified in Section 1.1 of the Supplementary Material.

2.6. Copper surface characterization

The Cu-mCans were recovered from the microcosms after 45 days of anoxic incubation, unscrewed, and left to dry under an anoxic atmosphere. Once dried, the bases of the Cu-mCans were coated with carbon using an EMITECH K975X evaporator. Then the samples were analyzed by high-resolution scanning electron microscopy (HRSEM) using an AURIGA Carl Zeiss SMT microscope, coupled with qualitative and quantitative energy dispersive X-ray (EDX) microanalysis.

In addition, chemical analysis using X-ray photoelectron spectroscopy (XPS) was conducted on the surface of the Cu-mCan lids (with no previous preparation) using a Kratos AXIS Supra photoelectron spectrometer following the procedure described by Martinez-Moreno et al. (2024b). The spectrum peaks were fitted by CasaXPS 2.3.22 software (Fairley, 2019). All binding energies were offset by referencing the adventitious carbon C1s peak (285 eV). No further constraints were applied to the initial binding energy values.

3. Results

3.1. Visual transformations of the microcosms over one-year anoxic incubation

The color transformation occurring in the microcosms throughout the incubation time is shown in Fig. 2. After 45 days, microcosms containing BPAS consortium (BC) showed a thin layer of reddish coloration at the bentonite:supernatant interface as well as accumulations in some of the samples in the bentonite phase (red arrows, Fig. 2). These red products shifted, or were masked, by gray-black hues over the incubation period. The formation of small fissures in the bentonite phase of the microcosms (white arrows, Fig. 2) and a characteristic smell of rotten eggs could be related to the gas generation.

The addition of the BPAS consortium (BC) in the microcosms stimulated the presence of reddish precipitates observed in the early stages (45 days) of incubation in the samples. Moreover, the addition of electron donors/acceptor (eD) also enhanced this color transformation, while heat-shocked bentonite treatment slowed it. Interestingly, in the sample of heat-shocked bentonite with Se (StB.Se), no visual color change was observed throughout the year of incubation (Fig. 2).

3.2. Dynamics of geochemistry over one-year incubation

The pH values in the microcosms exhibited alkaline to neutral values at the initial time (t. 0) gradually decreasing and stabilizing around 7.50–8.50 (depending on the treatment) after one year of incubation (t. 365) (Supplementary Fig. S2).

The percentage of lactate, acetate, and sulfate in the amended microcosms (eD) is shown in Fig. 3. Lactate showed a fast consumption (Fig. 3A). The depletion of this electron donor was particularly evident in the microcosms spiked with the BPAS consortium (B.eD.Se.BC), where total lactate depletion occurred within the first 45 days of incubation. This process exhibited a gradual slowdown in the absence of the BPAS consortium (B.eD.Se), followed by the heat-shocked bentonite microcosms with BPAS consortium (StB.eD.Se.BC), and lastly, those with heat-shocked bentonite (StB.eD.Se). In these last samples, complete lactate consumption was achieved before one-year incubation. As expected, lactate consumption exhibited a close correlation with acetate production in the microcosms (Fig. 3B). The rise in acetate content, along with subsequent consumption, was closely linked to lactate

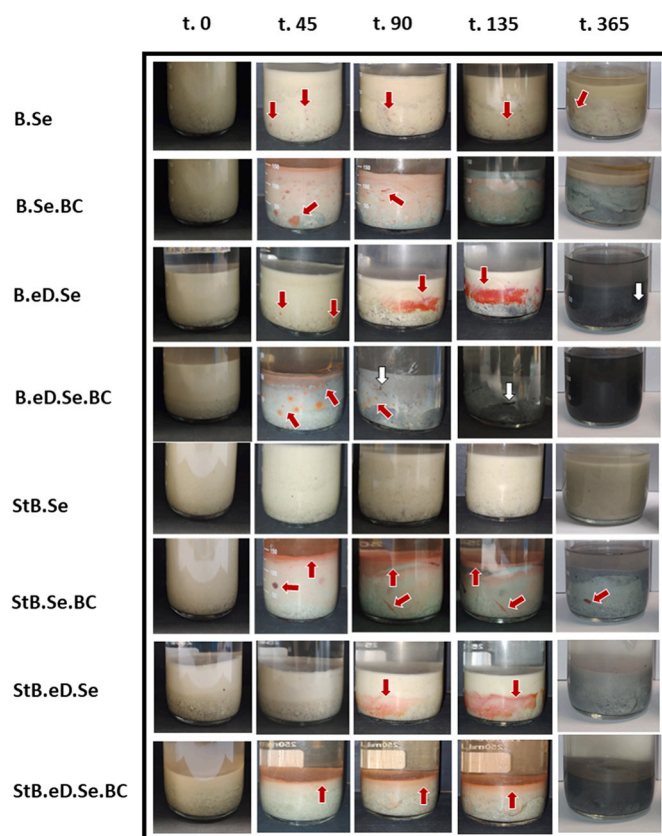


Fig. 2. Microcosms evolution over time of study (0, 45, 90, 135, and 365 days of incubation). Red arrows: precipitates attributed to Se(IV) reduction to Se(0). White arrows: fissures attributed to gas formation. Glossary: B: bentonite, StB: heat-shocked bentonite, eD: addition of electron donors/acceptor (ALS), Se: 2 mM of Se(IV), BC: spiked with BPAS consortium.

evolution, with the faster processes observed in the B.eD.Se.BC sample, followed by B.eD.Se, StB.eD.Se.BC, and StB.eD.Se.BC. It is noteworthy that, even after a year of incubation, acetate was not completely consumed in any of the treatments. Only the B.eD.Se.BC treatment approached complete acetate consumption before the end of the incubation year while, in the heat-shocked samples, the consumption of acetate was poorly detected (StB.eD.Se.BC) or only produced (StB.eD.Se). In the case of sulfate (Fig. 3C), its consumption was most pronounced in the non-heat-shocked samples containing the BPAS consortium. In the samples B.eD.Se, StB.eD.Se.BC, and StB.eD.Se, sulfate content remained relatively constant throughout the incubation time, slightly dropping after one year of incubation (consumption of $\approx 80\%$, 50% , 10% , respectively).

In summary, the progression of lactate consumption was intricately associated with acetate production and, to a lesser extent, to sulfate consumption. Furthermore, the addition of the BPAS consortium in the microcosms stimulated the mentioned processes, whereas tyndallization (heat-shock) of the bentonite hindered them.

3.3. Characterization of the microcosm's interface precipitates

As showed in Fig. 2, the reddish coloration was more pronounced and heterogeneously distributed in the samples spiked with the BPAS consortium (BC) after 45 days of incubation. In contrast, the process was slower in the absence of the BPAS consortium. For this reason, this early-stage of incubation was selected for the characterization of the resulting products.

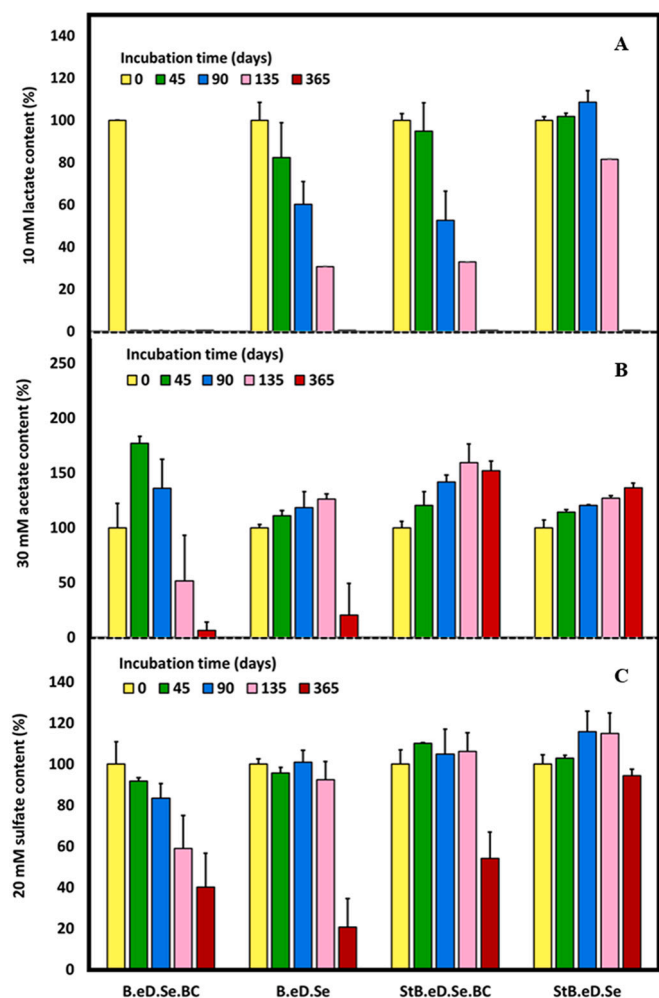


Fig. 3. Variations in the initial concentration of 10 mM lactate (A), 30 mM acetate (B), and 20 mM sulfate (C) of the electron donors/acceptor-amended treatments. Data include mean values along with standard deviations, calculated from each independent microcosm. Glossary: B: bentonite, StB: heat-shocked bentonite, eD: addition of electron donors/acceptor (ALS), Se: 2 mM of Se(IV), BC: spiked with BPAS consortium.

3.3.1. Microscopic and spectroscopic characterization

The study of the Se reduction products, morphology and elemental composition was determined by HAADF-HRTEM coupled with EDX maps, and their crystalline structure was achieved by SAED and lattice spacing measured using HRTEM. No red layer in the interface bentonite: supernatant at 45-days incubation was observed in the microcosms lacking the BPAS consortium (Fig. 2). In these samples, only bentonite was detected, as shown by the Si, Al, Fe, Mg signals in the microanalyses and the elemental distribution in the EDX maps (Supplementary Fig. S3).

In the consortium-containing samples (BC samples), thin sections of the interface layer showed the presence of electron-dense precipitates of different sizes, shapes and locations (Fig. 4). EDX analyses confirmed that these electron-dense accumulates corresponded to the formation of Se species (selenium reduction products, SeRPs). As indicated by the phosphorous (P) signal in the EDX maps (Fig. 4C), all BC-treatments showed intracellular selenium nanostructures or were found near cellular biomass with a rounded shape. SAED analysis (Fig. 4B) confirmed that these structures were amorphous (*a*-Se). In addition, extracellular SeRPs with different morphology and size were found in all samples (Fig. 4). The elemental mapping of these electron-dense precipitates (Fig. 4C) in each sample showed a composition of Se and sulfur (S). The SAED patterns (Fig. 4B) indicated the crystallinity of these

precipitates, while the lattice spacing observed at high resolution (Fig. 4D) showed values of 0.30 nm and 0.37 nm, corresponding to the (101) and (100) planes of trigonal selenium (*t*-Se), respectively; and 0.38 nm corresponding to (211) plane of monoclinic selenium (*m*-Se).

3.3.2. X-ray absorption (XAS) analysis

X-ray absorption spectroscopy (XAS) spectra of the SeRPs in the Se-containing treatments (B-Se.BC, B.eD.Se.BC, StB.Se.BC, and StB.eD.Se.BC) provided structural data on the oxidation state of Se and local coordination of this element within the studied treatments. The X-ray absorption near-edge structure (XANES) region revealed that Se(0) dominated the local coordination of Se (Fig. 5). This indicated that the whole amount of reduced Se in solid form consisted of Se in the zero-valent oxidation state. The extended X-ray absorption fine structure (EXAFS) spectra of the SeRPs and Se foil (Se⁰ reference compound) including their corresponding Fourier transforms (FT) and fit parameters of the calculated spectra are shown in Fig. 5 and Table 2, respectively. FT peak distances were uncorrected for scattering phase shift ($R + \Delta R$). The EXAFS fit spectra analysis of the four samples revealed a single Se—Se coordination shell, with N values ranging from 1.9 to 2.7 and a bond distance of approximately $2.33\text{--}2.35 \pm 0.0013\text{--}0.0026 \text{ \AA}$ (Table 1). The calculated bond distances were similar to those attributed to amorphous Se according to the literature ($2.33\text{--}2.34 \text{ \AA}$) (Eswayah et al., 2017; Ruiz-Fresneda et al., 2020; Povedano-Priego et al., 2023). The bond distance of the second Se—Se coordination shell ($3.63\text{--}3.70 \pm 0.02 \text{ \AA}$) would give insights on the crystalline Se, as indicated by Eswayah et al. (2017). However, after several attempts, it failed due to the small amplitude of this peak in the four studied samples.

3.4. Analysis of microbial communities

Total DNA was extracted and sequenced from the bentonite of the microcosms after 45 days of incubation (where the microcosms exhibited greater visual heterogeneity between treatments). The samples B.Se.BC_R1 and StB.eD.Se_R1 were not included in this study due to their failure during the DNA extraction step. A total of 353 phylotypes were annotated in 12 phyla (98.34 %) being the most abundant *Pseudomonadota* (68.00 %) and *Bacillota* (26.58 %) (Supplementary Table S2). At the genus level, 135 OTUs were annotated as *Pseudomonas* (40.30 %), *Stenotrophomonas* (12.52 %), *Symbiobacterium* (12.43 %), unclassified *Clostridia* (6.93 %), unclassified *Rhodospirillales* (6.00 %), and *Pseudoalteromonas* (2.79 %) showing the higher relative abundance in the pool of samples (Supplementary Table S3).

The principal coordinate analysis (PCoA) represented the dissimilarity between the samples spiked with (BC samples) and without the BPAS consortium. Within BC samples (PCoA with this subset of samples, Fig. 6), no difference was observed between heat-shocked (StB) and non-heat-shocked (B) bentonite. However, in the treatments without BPAS consortium, the dissimilarity between heat-shocked bentonite (StB) and non-heat-shocked bentonite (B) was evidenced (Fig. 6).

To identify the OTUs involved in the dissimilarity between samples, a heatmap was constructed (Fig. 7). In the absence of BPAS consortium in the heat-shocked bentonite samples (StB cluster, green bracket Fig. 7), bacterial diversity significantly diminished compared to that of the other treatments. The marked differentiation in these treatments was due to the abundance of *Pseudomonas*, *Symbiobacterium*, *Stenotrophomonas*, and unclassified *Clostridia*. Concerning the samples spiked with the BPAS consortium (BC cluster, purple bracket Fig. 7), the observed group was in line with expectations, as it was attributed to the bacterial genera inherent to the consortium, such as *Pseudomonas*, *Stenotrophomonas* and, to a lesser extent, *Amycolatopsis*. In the cluster of non-heat-shocked bentonite (B cluster, brown bracket Fig. 7), the abundance of unclassified *Clostridia*, unclassified *Rhodospirillales*, *Pseudoalteromonas*, *Noviherbaspirillum*, and, to a lesser extent, *Pseudomonas*, marked the dissimilarity from the other treatments.

The alpha-diversity indices of the treatments (duplicates in B.Se.BC

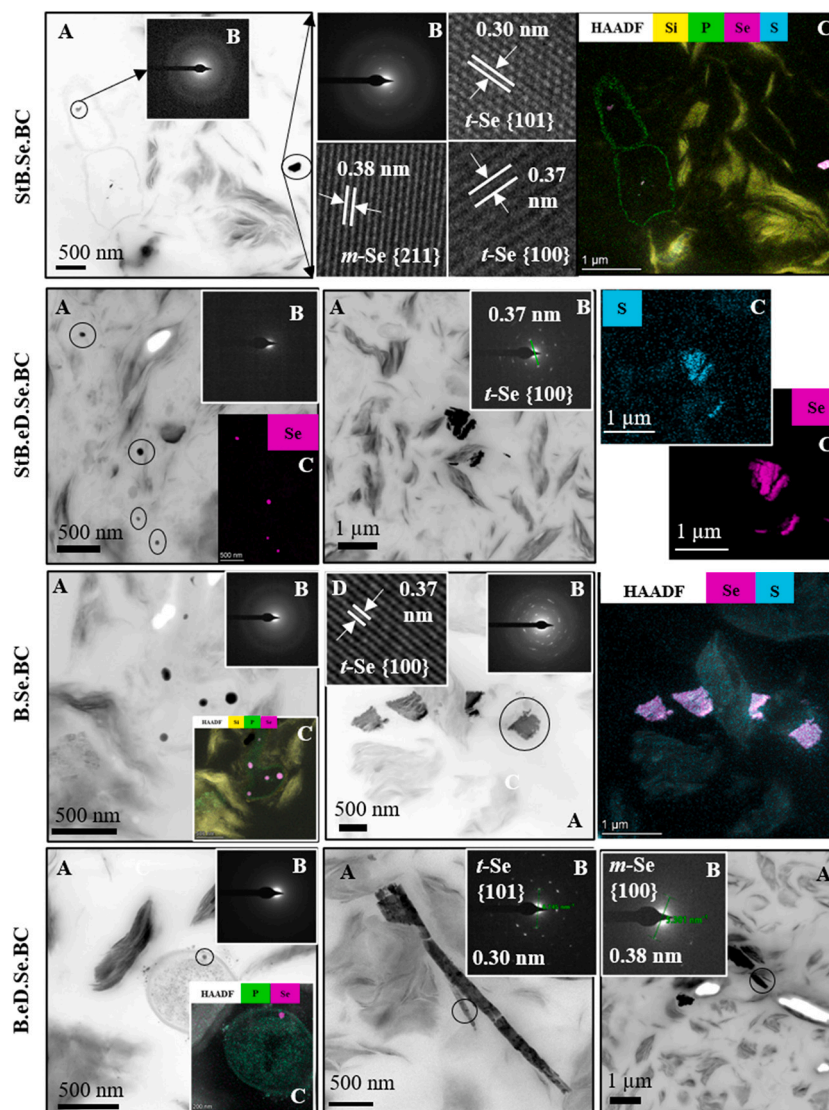


Fig. 4. HRTEM micrographs of the SeRPs from the BC microcosms at 45 days of incubation. A) HAADF images, B) associated SAED patterns, C) EDX maps showing the elemental distribution of Si, P, Se, Fe, and S; D) high resolution images and d-spacing. Glossary: B: bentonite, StB: heat-shocked bentonite, eD: addition of electron donors/acceptor (ALS), Se: 2 mM of Se(IV), BC: spiked with BPAS consortium.

and StB.eD.Se) at the genus level are shown in Supplementary Table S4. The richness index (Sobs) of the non-heat-shocked samples (B samples) showed higher values in the treatments without BPAS consortium (BC), particularly higher values in the absence of electron donors/acceptor (B.Se > B.eD.Se > B.eD.Se.BC > B.Se.BC). In contrast, the samples with heat-shocked bentonite (StB samples) exhibited a different trend. The richness indices were higher in the treatment with electron donors/acceptor, followed by samples spiked with the BPAS consortium, the treatment with selenium only, and finally, the samples amended with electron donors/acceptor and the BPAS consortium (StB.eD.Se > StB.Se.BC > StB.Se > StB.eD.Se.BC). Regarding the diversity values, the treatments with non-heat-shocked bentonite (B.Se) had the highest values, followed by the samples amended with electron donors/acceptor (B.eD.Se), whose ShannonH and SimpsonD values were greater than 3 and close to 1, respectively. The remaining treatments exhibited lower values, with ShannonH lower than 3 (1.37–2.36) and SimpsonD further from 1 (0.39–0.64) (Supplementary Table S4). These values suggested reduced diversity in the latter samples and the potential genus dominance in the microcosms.

The relative abundance of OTUs in each treatment in triplicate (duplicates in B.Se.BC and StB.eD.Se) are shown in Fig. 8 and

Supplementary Table S3. Overall, *Pseudomonas* emerged as the predominant OTU in this study across the sample pool (40.30 % of the total relative abundance). Its dominance was particularly pronounced in samples spiked with the BPAS consortium (BC samples), where it constituted the taxa dominance in the community, ranging from 77.20 % of relative abundance in sample B.Se.BC to 48.18 % in sample B.eD.Se.BC. Within this subset of samples, *Stenotrophomonas* (member of the BPAS consortium) emerged as the second most represented genus, with relative abundance ranging from 34.47 % in sample B.eD.Se.BC to 10.79 % in sample B.Se.BC. The relative abundance of *Amycolatopsis* in the BC treatments was comparatively lower than the other members of the consortium, ranging between 4.63 % in sample B.eD.Se.BC and 0.38 % in sample B.Se.BC. Conversely, *Bacillus* was absent possibly for sequencing limitations.

Regarding samples lacking the BPAS consortium (B.eD.Se and B.Se), the OTU with the highest relative abundance was unclassified Rhodospirillales (23.18 % and 20.65 %, respectively). This group was followed by unclassified Clostridia (23.14 %), *Desulfosporosinus* (9.05 %), and *Pseudomonas* (8.89 %) in sample B.eD.Se. In the case of B.Se, the following most abundant OTUs were *Pseudoalteromonas* (19.11 %), unclassified Clostridia (13.94 %), and *Noviherbaspirillum* (8.55 %). The

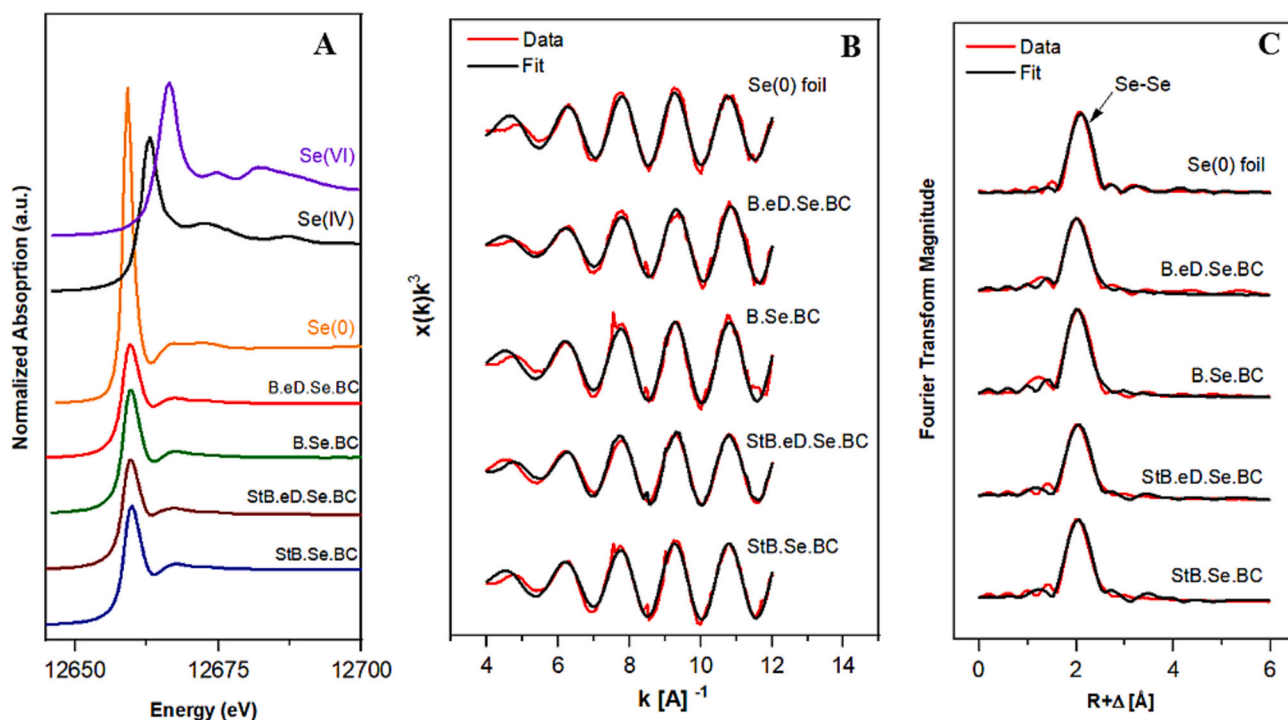


Fig. 5. (A) XANES spectra of Se reference compounds Na_2SeO_3 (Se^{IV}), Se foil (Se^0), and Na_2SeO_4 (Se^{VI}), and SeRPs from B.eD.Se.BC, B.Se.BC, StB.eD.Se.BC and StB.Se.BC samples after 45 days of incubation. (B) EXAFS spectra of Se foil and SeRPs from the microcosms and (C) their corresponding FT. Glossary: B: bentonite, StB: heat-shocked bentonite, eD: addition of electron donors/acceptor (ALS), Se: 2 mM of Se^{IV} , BC: spiked with BPAS consortium.

Table 2

EXAFS structural parameters of the Se foil and the selenium reduction products (SeRPs) from the selected Se-amended microcosms after 45 days of incubation.

Sample	Shell	N^d	R^b [Å]	σ^{2c} [Å ²]	ΔE [eV]
Se foil	Se-Se	3.2 ± 0.2	2.37	0.0040	-10.10
B.eD.Se.BC	Se-Se	1.9 ± 0.2	2.33	0.0013	-13.70
B.Se.BC	Se-Se	2.7 ± 0.2	2.34	0.0026	-12.37
StB.eD.Se.BC	Se-Se	2.4 ± 0.1	2.35	0.0024	-11.10
StB.Se.BC	Se-Se	2.5 ± 0.1	2.35	0.0025	-11.60

Glossary: B: bentonite, StB: heat-shocked bentonite, eD: addition of electron donors/acceptor (ALS), Se: 2 mM of Se(IV), BC: spiked with BPAS consortium.

^a Errors in coordination numbers are $\pm 25\%$ and standard deviations as estimated by EXAFSPAK.

^b Errors in distance are ± 0.02 Å.^c Debye–Waller factor.

bacterial diversity present in the microcosms was not greatly affected by the addition of electron donors/acceptor. However, there were some differences observed. Sample B.eD.Se had a higher presence of *Desulfosporosinus* and *Alkalihalobacillus* (9.05 % and 8.52 %, respectively) compared to B.Se (1.07 % and 0.21 %). On the other hand, *Pseudalteromonas* was more prominent in sample B.Se (19.11 %) than in B.eD.Se (0.21 %).

3.5. Microscopic and spectroscopic characterization of the Cu-mCan's surface

To evaluate the impact of microbial communities and the presence of selenium on the copper material after 45-day incubation, one Cu-mCan was collected from each microcosm. The surfaces underwent microscopic and spectroscopic analyses by HRSEM, EDX, and XPS. The copper surface characterization was focused on Cu-mCan recovered from non-heat-shocked bentonite microcosms.

Fig. 9 presents Cu-mCan and HRSEM images before (t. 0) and after a 45-day anaerobic incubation. Visual differences in coloration were

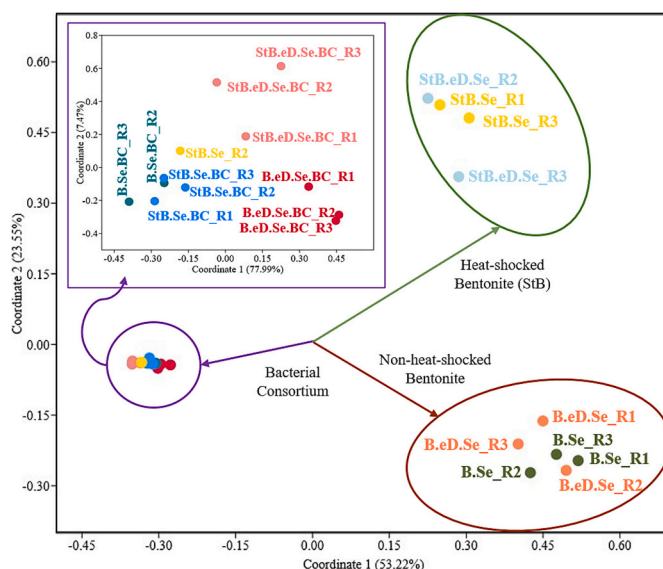


Fig. 6. Principal coordinate analysis (PCoA) comparing the bacterial communities at genus level from Se(IV)-containing microcosms after 45 days of incubation. Glossary: B: bentonite, StB: heat-shocked bentonite, eD: addition of electron donors/acceptor (ALS), Se: 2 mM of Se(IV), BC: spiked with BPAS consortium.

observed compared to the initial state of Cu-mCan (t. 0). It is worthy to note that the bentonite adhering to the copper surface was intentionally retained to prevent potential displacement of copper alteration related compounds. The sample B.eD.Se.BC showed a significant shift towards dark gray-black coloration (Fig. 9B). That hue was also observed in some regions of B.Se.BC and B.eD.Se (Fig. 9C and D). At the microscopic level, the post-incubation samples exhibited heterogeneous topography (second column, Fig. 9), in contrast to the uniformity observed in the t.

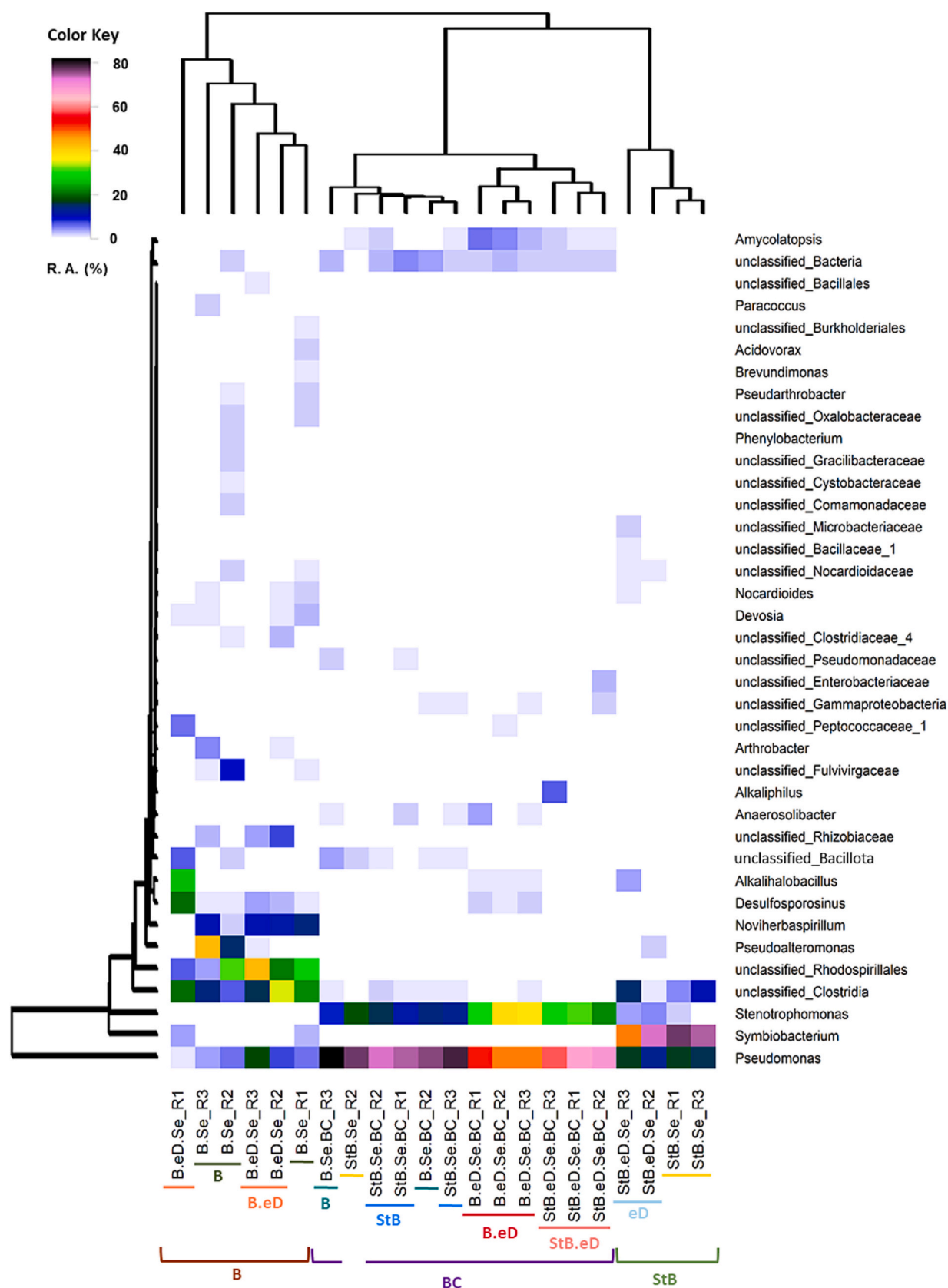


Fig. 7. Heatmap showing the bacterial relative abundance and clustering at genus level of the microcosms after 45 days of incubation. Cut-off: 1.33 % based on the maximums. The warmer the color, the greater is the relative abundance. The colored lines in X axis represent the clustering observed in PCoA. Glossary: B: bentonite, StB: heat-shocked bentonite, eD: addition of electron donors/acceptor (ALS), Se: 2 mM of Se(IV), BC: spiked with BPAS consortium.

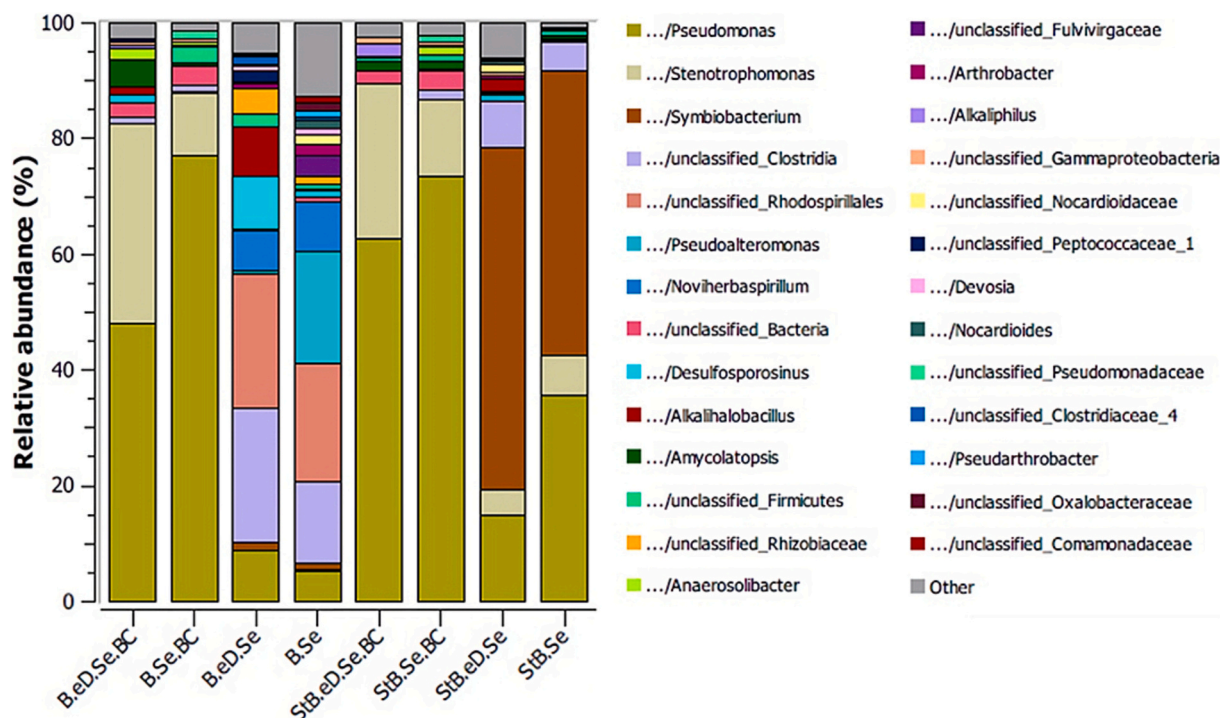


Fig. 8. Bacterial community structure within the bentonite microcosms showing the OTU relative abundance (averages of biological replicates) at genus level. Cut-off: 0.20 %. Glossary: B: bentonite, StB: heat-shocked bentonite, eD: addition of electron donors/acceptor (ALS), Se: 2 mM of Se(IV), BC: spiked with BPAS consortium.

0 sample. Cu-mCan at t. 0 only showed the presence of Cu and C in the EDX maps. The presence of C was attributed to the carbon metallization process during sample preparation for HRSEM. In addition, the subsequent columns of Fig. 9 present elemental EDX maps that illustrate the distribution of iron (Fe), aluminum (Al), sulfur (S), silicon (Si), oxygen (O), copper (Cu), and carbon (C) in selected areas. The Si (pink), Fe (yellow), and Al (cyan) signals were assigned to the residual bentonite adhered to the Cu surface. The signal of O (red) was mainly related to Si (Si—O bonds), indicating its presence within the bentonite. Additionally, to a lesser extent, O was detected on the surface of the copper.

Sample B.eD.Se.BC showed sulfur accumulates, which may be associated with copper corrosion (Cu_2S) (Fig. 9B) linked with the consumption of sulfate ($\approx 8\%$) (Fig. 3). The sample B.Se.BC also showed S-accumulates (Fig. 9C). However, in samples B.eD.Se and B.Se no sulfur was observed, and the detection of O was mainly related to the presence of bentonite (Fig. 9E and D). On the surface of these Cu-mCan, some “patches” were observed. Upon closer examination at higher magnification, these patches appeared to indicate some delamination on the copper surface, potentially exposing bare Cu to new oxidation processes (Fig. 9D, orange square). No Se signal was detected on the copper surface by EDX.

Additionally, XPS wide scans of the copper lids indicated the presence of Cu, C, O, Si, Na, Fe, Mg, and Al on all Cu-mCan surfaces. These elements (excluding copper) were attributed to the residual bentonite present on the copper surfaces. The high-resolution scans by XPS (Fig. 10) of the Cu 2p region revealed the presence of elemental copper on all sample surfaces, indicated by the peaks at 932.6 eV and 952.3 eV (Wagner et al., 1979; Mansour, 1994). Additional peaks at 933.6 eV and 953.70 eV evidenced the presence of CuO on all the samples (Ghijzen et al., 1988; Jolley et al., 1989), and the satellite peaks at around 942 eV and 962 eV were assigned to the presence of Cu^{2+} (Biesinger, 2017). It should be noted that, although the intensity of the Se signal in some of the scanned copper lids was low, given the low concentration expected for this element on the surface of the copper, the presence of Se was still evident in all the samples. The high-resolution scans of the Se 3d region

(Fig. 10) showed two peaks in all samples: a signal around 58.2 eV, which has been previously reported for Se(IV) from Na_2SeO_3 (Moulder et al., 1992), and another around 54.8 eV, usually attributed to Se(0) (Weser et al., 1977). The presence of both peaks indicates the reduction of Se(IV) to Se(0). In the microcosms with electron donors, the peaks of both Se(IV) and Se(0) could be clearly appreciated, but the intensity of Se(IV) and Se(0) are different. While the Se(IV) was evident, the peak corresponding to Se(0) was much more intense and defined, with the possibility of distinguishing the contributions from Se $3d_{3/2}$ and Se $3d_{5/2}$ separately. For example, in sample B.eD.Se the signal for Se(0) $3d_{3/2}$ appeared at 55.10 eV, and the peak for Se(0) $3d_{5/2}$ appeared at 54.24 eV. The separation between these two signals at 0.86 eV is in agreement with previously reported XPS Se spectra (Moulder et al., 1992).

4. Discussion

4.1. Microcosms evolution and dynamics of the water geochemistry

The visual color changes of the microcosms over one year of anoxic incubation showed a thin layer of reddish coloration at the interface and accumulations of reddish spots in the bentonite phase. This coloration is an indicator of the reduction of selenite [Se(IV)] to elemental selenium [Se(0)] (Povedano-Priego et al., 2023; Ruiz-Fresneda et al., 2018). These red Se(0) reduction products (SeRPs) shifted, or were masked by gray-black hues over the incubation period in the observed microcosms. This shift towards darker hues could be attributed to factors such as a transition in the Se allotropy of the SeRPs to more stable forms, or to the generation of the bacterial-produced H_2S , which can react with iron resulting in black precipitates of reduced iron species (Ruiz-Fresneda et al., 2023b; Miettinen et al., 2022; Matschiavelli et al., 2019). The formation of small fissures in the bentonite phase of the microcosms (white arrows, Fig. 2) and the characteristic smell of rotten eggs could be related to the gas generation (e.g., sulfide) mediated by bacterial activity (He et al., 2011). However, further investigations would be needed to determine the gases composition. It should be noted that the addition of

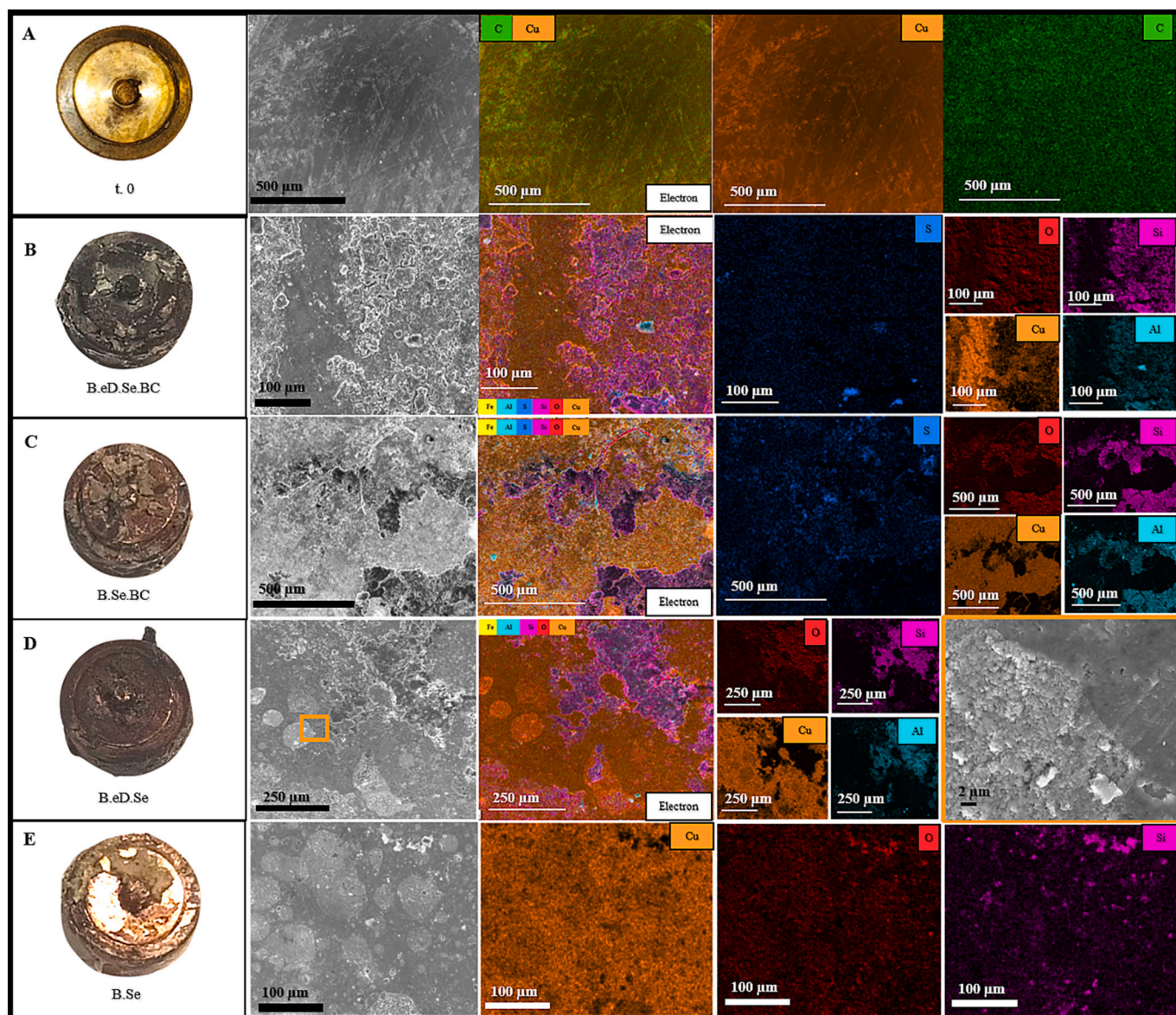


Fig. 9. Visual images (first column), electron images, and EDX maps of the Cu-mCan surface before experimental set-up (A) and after 45-days incubation from treatments B.eD.Se.BC (B), B.Se.BC (C), B.eD.Se (D), and B.Se (E). EDX maps show the distribution of Cu (orange), Fe (yellow), S (dark blue), Si (pink), Al (cyan), O (red), and C (green) in the studied area. Glossary: B: bentonite, StB: heat-shocked bentonite, eD: addition of electron donors/acceptor (ALS), Se: 2 mM of Se(IV), BC: spiked with BPAS consortium.

the BPAS consortium (BC) in the microcosms promoted Se reduction process, with reddish coloration observed at 45-days incubation. The addition of electron donors/acceptor (eD) also enhanced the reduction process, while bentonite heat-shock slowed down this color shift. Regarding the sample of heat-shocked bentonite with Se (StB.Se), no visual color transition was apparent throughout the year of incubation indicating no Se(IV) reduction either alteration to darker hues in the bentonite. Since tyndallization is not the most effective process for bentonite sterilization (Martinez-Moreno et al., 2024a), it was observed that, under the studied conditions, this process can however influence bacterial activity.

Regarding the dynamic in the water geochemistry, the pH values in the microcosms over the course of incubation exhibited a tendency to become less alkaline, stabilizing within neutral values. This trend was in accordance with previous studies without Se conducted by Martinez-Moreno et al. (2024b) where indicated that the observed trend in the pH might be related to the ionic exchange occurring between bentonite and the different solvents (e.g., acetate, lactate, sulfate, and the EW) and/or

the gas generation induced by the microbial communities' metabolisms. However, the addition of 2 mM of Se(IV) did not impact the pH trend of the microcosms. The progression of lactate consumption was intricately associated with acetate production and, to a lesser extent, to sulfate consumption. Furthermore, the addition of the BPAS consortium in the microcosms stimulated the consumption and/or production of lactate, acetate and sulfate, whereas the heat-shock of the bentonite hindered them. This dynamic was also observed in Martinez-Moreno et al. (2024b) with an important difference: the presence of Se(IV) slowed the dynamics of the electron donors/acceptor. In the cited work, the authors proposed that microorganisms could use lactate, without sulfate reduction, through lactate fermentation pathway, which results in the production of acetate and propionate, or by the incomplete oxidation of lactate to acetate coupled with the reduction of iron (Park et al., 2024). Additionally, the decrease in sulfate content observed in the treatment B.eD.Se.BC may be due to the sulfate reduction to hydrogen sulfide with the concurrent incomplete oxidation of lactate to acetate through the reductive pathway of acetyl-CoA (Matschiavelli et al., 2019). This last

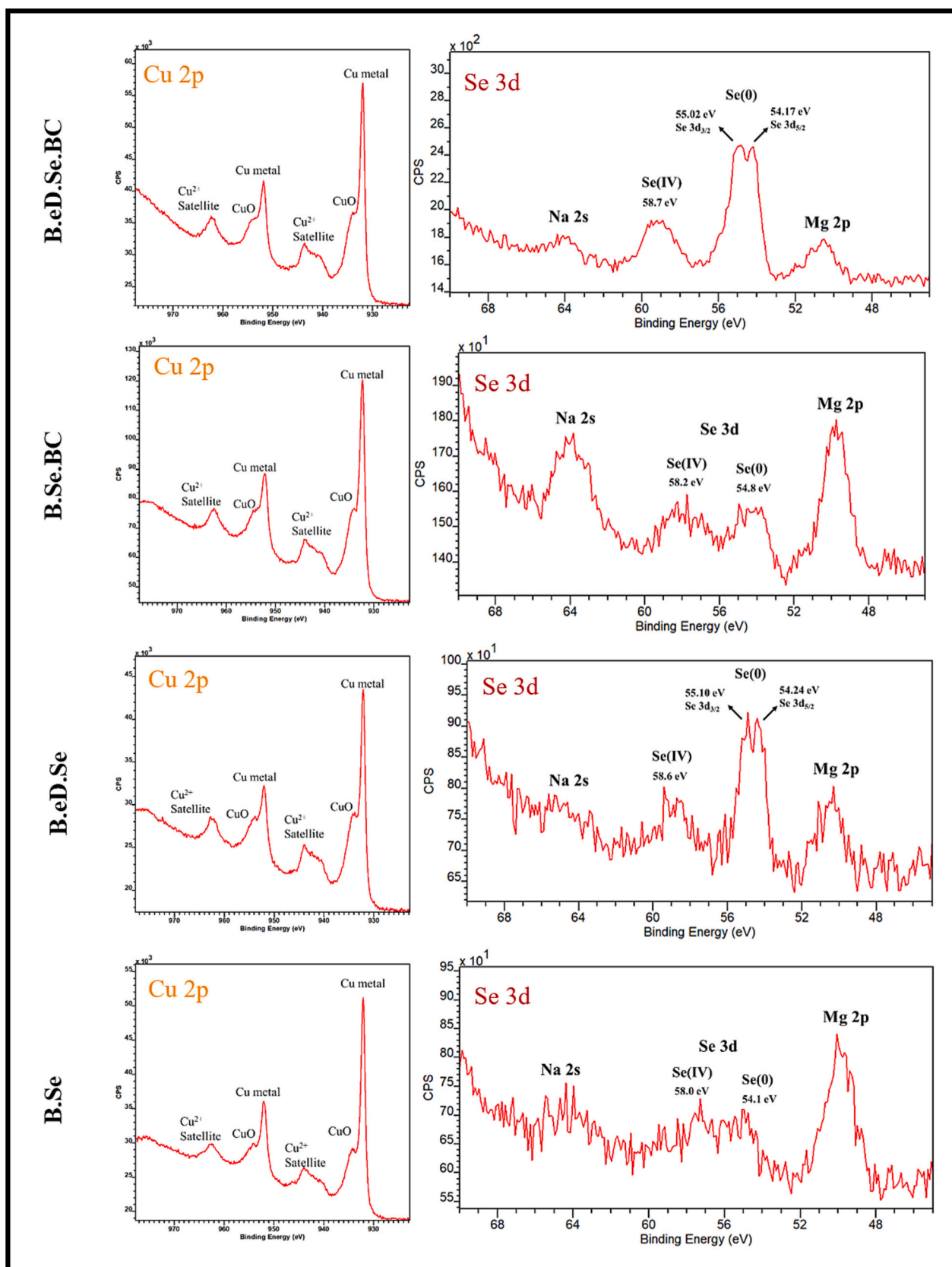


Fig. 10. High-resolution XPS spectra of the regions Cu 2p (977 eV – 922 eV) and Se 3d (70 eV – 45 eV) of the copper surface recovered from the microcosms after 45-days incubation. Glossary: B: bentonite, StB: heat-shocked bentonite, eD: addition of electron donors/acceptor (ALS), Se: 2 mM of Se(IV), BC: spiked with BPAS consortium.

component formation could be related to the fissures observed in the microcosms (Fig. 2) and the rotten egg odor after sampling (He et al., 2011). It is noteworthy that, even after a year of incubation, acetate was not completely consumed in any of the treatments. Only the B.eD.Se.BC treatment approached complete acetate depletion before the end of the incubation. This finding demonstrated the negative impact of the Se(IV) addition on the activity of the bacterial community slowing the consumption/production of lactate, acetate, and sulfate compared to Se(IV)-untreated microcosms described in Martinez-Moreno et al., 2024b.

The presence of Se(IV) at 2 mM can be toxic to some bacteria (Povedano-Priego et al., 2023) and might reduce the bacterial activity within the microcosms. Moreover, this metalloid could act as a competitor of sulfur as a final electron acceptor under anaerobic condition (Staicu and Barton, 2021) associated to the slow consumption in the microcosms (Fig. 3C). This fact was observed comparing samples B.eD.Se.BC and B.eD.Se, where sulfate consumption was lower in the presence of the BPAS consortium showing the preference of those bacteria to use selenite as electron acceptor within a detoxification process instead of sulfate. The presence of Se(IV) could lead to a deceleration of biogeochemical processes, attributed to a reduction in bacterial diversity and/or an extended adaptation period for selenium-tolerant microorganisms.

4.2. Effect of Se(IV) addition on the microbial communities in the early-incubation stage

Comparing the relative abundances of the bacterial strains from the BPAS consortium (*Bacillus*, *Pseudomonas*, *Amycolatopsis* and *Stenotrophomonas*) in this study with those microcosms without Se(IV) from the previous study by Martinez-Moreno et al. (2024b), several differences were noted. In the presence of Se(IV), *Pseudomonas* decreased from 69.53 % to 48.18 %, and from 78.88 % to 77.20 % in B.eD.Se.BC and B.Se.BC treatments, respectively, compared to its counterpart without Se(IV). Conversely, in the heat-shocked bentonite (StB) treatments, *Pseudomonas* increased from 57.73 % to 62.80 %, and from 54.59 % to 73.44 % in StB.eD.Se.BC and StB.Se.BC treatments, respectively, compared with the samples without Se detailed in Martinez-Moreno et al. (2024b). For *Stenotrophomonas*, the addition of Se(IV) increased its abundance from 8.12 % to 34.47 % in B.eD.Se.BC treatment compared to B.eD.BC, while it decreased from 34.96 % to 13.24 % in StB.Se.BC treatment compared to StB.BC. *Amycolatopsis* showed a higher abundance (from 2.31 % to 4.63 %) in B.eD.Se.BC, and was detected in StB.Se.BC at 1.21 %, compared to its absence in the Se(IV)-free counterpart.

The effect of Se(IV) addition in the microcosms appears to have a potentially negative or positive impact on the BPAS consortium members depending on the treatment and the bacterium. This effect is compensated by a balanced increase-decrease in *Pseudomonas* and *Stenotrophomonas*, which were the dominant genera in the spiked microcosms. *Pseudomonas* and *Stenotrophomonas* have demonstrated tolerance and the ability to interact with Se(IV) by reducing it to Se(0) under anoxic conditions, resulting in the formation of orange-reddish precipitates in form of selenium nanoparticles (SeNPs) (Staicu et al., 2015; Ruiz-Fresneda et al., 2019). This process is linked to the presence of red precipitates observed in the microcosms spiked with BPAS consortium at 45 days-incubation (BC microcosms, Fig. 2). The presence of the BPAS consortium stimulated the Se(IV) reduction processes since in the unspiked treatments, the reddish precipitates were less evidenced after 45 days of incubation (Fig. 2). These bacteria have demonstrated the capacity to metabolize acetate and/or lactate as a carbon source under anoxic conditions (Freikowski et al., 2010; Sanchez-Castro et al., 2017) and could play an important role in the lactate consumption and acetate production observed after 45 days of incubation in the BC treatments (Fig. 3).

In samples lacking the BPAS consortium (B.eD.Se and B.Se), the presence of Se(IV) caused shifts in bacterial community composition compared to its counterparts without Se(IV) observed by Martinez-

Moreno et al. (2024b). Following the results observed in the mentioned study, the addition of Se(IV) eliminated the presence of *Desulfocurvibacter* and *Desulfuromonas* in B.eD.Se and B.Se. Additionally, electron donors/acceptor had minimal effect on bacterial diversity. Treatment B.eD.Se showed higher levels of *Desulfosporosinus* and *Alkalihalobacillus* compared to B.Se. Conversely, *Pseudalteromonas* was more abundant in B.Se than in B.eD.Se.

Desulfosporosinus is a SRB capable of reducing sulfate via incomplete oxidation of lactate resulting in the production of acetate and CO₂ (Stackebrandt et al., 1997), and may be one of the bacteria involved in the slight production of acetate observed at 45-days incubation in the B.eD.Se sample (Fig. 3). In addition, their tolerance to the presence of Se was previously demonstrated (Povedano-Priego et al., 2023; Aoyagi et al., 2021). Additionally, *Alkalihalobacillus* is a recently described genus with some members being facultative anaerobic and tolerant to heavy metals and metalloids such as chromium or arsenic, which may be associated to the tolerance to Se(IV) (Patel and Gupta, 2020; Gautam et al., 2022; Haghi et al., 2023). Regarding the heat-shocked bentonite treatments without the BPAS consortium (StB.eD.Se and StB.Se), it is worth noting the high relative abundance of *Symbiobacterium* (58.97 % and 49.21 %, respectively). This anaerobic bacterium can grow in temperatures ranging from 40 to 70 °C (Shiratori-Takano et al., 2014). Previous studies have identified this genus with an important relative abundance in selenite-containing soils (Povedano-Priego et al., 2023; Aoyagi et al., 2021).

Overall, the presence of Se(IV) influenced the bacterial communities within the microcosms. Therefore, it is important to explore these communities' role in the interaction with this metalloid and its impact on Se speciation.

4.3. Characterization of the selenium reduction products (SeRPs)

In order to elucidate the first steps of Se(IV) reduction, this section is focused, as previously mentioned, on an early-stage (45-day incubation) characterization of the selenium reduction products (SeRPs). At this incubation time, Se reduction was more pronounced in the samples containing the BPAS consortium (BC samples). The ability of the BPAS strains to reduce Se(IV) to Se(0) has been previously reported by Povedano-Priego et al. (2023), where these bacteria promoted Se(IV) reduction resulting in the production of nanoparticles of Se(0). Furthermore, the predominant bacteria in the BC-containing microcosms of this study, *Pseudomonas* and *Stenotrophomonas*, were the most abundant genera (Fig. 8), which showed the ability to tolerate selenium through its reduction to Se(0) nanoparticles (Staicu et al., 2015; Ruiz-Fresneda et al., 2019). In addition to biotic factors, Se(IV) immobilization can be mediated by abiotic processes (Wang et al., 2022). These abiotic processes include the adsorption of Se to the surface of clay minerals, its reduction to elemental Se mediated by pyrite (FeS₂) oxidation, or via structural Fe(II) present in smectites (Hoving et al., 2019; Kang et al., 2011; Breynaert et al., 2010). In contrast, no abiotic reduction of selenite was detected in our study (sample StB.Se, Fig. 2 and Supplementary Fig. S1).

Selenium can manifest in three different allotropes: amorphous (*a*-Se), monoclinic (*m*-Se), and trigonal (*t*-Se), with *a*-Se considered thermodynamically unstable, while *t*-Se represents the most stable allotrope. The structural analysis of the SeRPs in this study unveiled that intracellular selenium precipitates, in form of nanoparticles (SeNPs), exhibited amorphous allotropy. In contrast, extracellular electron-dense aggregates were identified as SeRPs with monoclinic and trigonal allotropy, occasionally combined (sample StB.Se.BC, Fig. 4). Notably, the extracellular crystalline SeRPs demonstrated a close association with sulfur (S), as evidenced in the EDX maps (Fig. 4C). This suggested that the reduction of Se(IV) to Se(0) might occur within the bacterial cells, resulting in the formation of amorphous SeNPs (*a*-Se). Subsequently, these particles could be released into the extracellular environment through mechanisms such as cellular detoxification or lysis. Once in the

extracellular space, the transformation process to *m*-Se and, subsequently, to *t*-Se would take place. This finding aligned with those of previous research involving complex saturated-bentonite microcosms under anaerobic conditions (Povedano-Priego et al., 2023) and supported the mechanism proposed by Ruiz-Fresneda et al. (2018). XAS was used to get insights into the local coordination of Se within the samples (e.g., Se—Se bond distances) which help to determine the proportion of different Se allotropes. The EXAFS fit analysis indicated that Se(0) is mainly present as amorphous form where a Se—Se bond distance is observed, slightly lower than that of the trigonal Se allotrope (Se—Se bond distance ≈ 2.37 Å). Since EXAFS is a bulk technique, no solid structure evidence for the transformation of *a*-Se to *t*-Se was detected as suggested by STEM/HAADF. However, low proportion of *t*-Se is not discarded in the studied samples.

Moreover, the presence of sulfate in the microcosms could mediate the interaction of the SeNPs with S to form the observed selenium-sulfur precipitates in the extracellular environment (Vogel et al., 2018). The Se—S interaction manifested as precipitates may impede sulfate availability that could impact the corrosion of copper material. It is crucial to explore not only its influence on bacterial communities but also how the presence of Se(IV) in the microcosms might affect the microbial-influenced corrosion of Cu-mCan.

4.4. Chemistry of the copper surface

The signal of Se(0) detected by XPS on the copper surface, showed its highest intensity in the sample B.eD.Se.BC, indicating that the addition of electron donors/acceptor and the BPAS consortium presented the highest effect in the Se reduction processes. According to the literature, Cu_2S is expected to exhibit a Cu $2p_{3/2}$ peak around 932 eV (Fig. 10), although confirming the presence of this compound is challenging because this signal would be overshadowed by the elemental Cu peaks (Gebhardt et al., 1986; Romand et al., 1978). Nonetheless, as stated in Martínez-Moreno et al. (2024b), the presence of S-aggregates observed by microscopy (Fig. 9) on the copper surface of treatment B.eD.Se.BC and B.Se.BC might be related to the presence of Cu_2S resulted from microbial activity. Still, additional techniques should be carried out to better understand the speciation of the S-aggregates.

The use of lactate as electron donor by SRB coupled to the reduction of sulfate to sulfide under anoxic conditions can occur via dissimilatory sulfate reduction pathway (Dou et al., 2020). Moreover, Salehi Alaei et al. (2023) reported that the transformation of copper oxide (Cu_2O) into copper sulfide (Cu_2S) through a chemical exchange with sulfide could be thermodynamically possible. In addition, the formed HS^- , resulting from the SRB metabolite H_2S , could migrate to the copper surface and react with it leading to the formation of Cu_2S (Dou et al., 2020).

SRB could bind to copper surfaces creating a primary corrosion film of Cu_2S (Chen et al., 2014). The creation of this Cu_2S film and the production of extracellular polymeric substances (EPS) by SRB can reduce the toxicity of copper (from the canister surface) to this group of bacteria. Moreover, the presence of SRB has been proven to cause high-purity copper corrosion in groundwater boreholes or MX-80 clay, leading to Cu_2S precipitate formation (Johansson et al., 2017; Masurat et al., 2010). In a recent study, Martínez-Moreno et al. (2023) demonstrated that the addition of acetate, lactate, and sulfate in bentonite blocks compacted to a high dry density stimulated bacterial activity, resulting in the formation of small corrosion compounds on the surface of copper disks. In the present work, the high presence of water accelerated the corrosion processes and the formation of precipitates was observed as early as 45 days of incubation.

5. Conclusions

Visually, the addition of the BPAS consortium in the microcosms promoted the processes of Se(IV) reduction to Se(0), followed by the

addition of electron donors/acceptor. In contrast, the tyndallization (heat-shock) of the bentonite delayed these processes, with no selenium reduction (red color) detected in the StB.Se sample over the year of incubation. The addition of Se(IV) affected microbial-mediated biogeochemical process due to its toxicity for some bacteria within the bentonite community. On the other hand, the presence of nutrients such as lactate, acetate and sulfate stimulated microbial activity.

The presence of Se(IV) in the microcosms reduced the presence of some SRB, while the electron donors/acceptor stimulated the growth of the Se-tolerant SRB *Desulfosporosinus*. Additionally, Se-tolerance bacteria such as *Pseudomonas*, *Stenotrophomonas*, and *Alkalibacillus* may contribute to the visual evolution in the microcosms, indicated by the evidence of Se(IV) reduction to Se(0) over the year-long anaerobic incubation period. In samples with electron donors/acceptor, lactate was the main carbon source to be consumed, associated with acetate production and subsequent consumption, and to a lesser extent, sulfate reduction. The dynamic rate of these processes in the samples increased upon the nature of the biological of physicochemical parameter in the following order: spiked BPAS consortium > amended electron donors/acceptor > bentonite heat-shock.

The presence of the BPAS consortium revealed the reduction of selenium. The suggested process started with the intracellular uptake and reduction of Se(IV) to Se(0) in form of nanospheres with amorphous allotropy (*a*-Se), which in the extracellular space, led to the transformation of extracellular crystalline structures, progressing from monoclinic selenium (*m*-Se) and concluding with the most stable form of trigonal selenium (*t*-Se).

SRB oxidized lactate by using sulfate as final electron acceptor via dissimilatory pathway. The resulting biogenic sulfide may participate in a chemical substitution with copper oxides, which could be the result of the presence of oxygen that has been trapped in the bentonite or the reduction of H_2O molecules, resulting in the formation of copper sulfide (Cu_2S). Moreover, HS^- could react with copper surface and deal with the formation of Cu_2S precipitates. However, further analyses are required to investigate the impact of Se(IV) on copper biocorrosion.

Overall, the presence of Se(IV) impacted the bacterial communities inherent of the Spanish bentonite by affecting their activity. Furthermore, the enrichment of selenium-tolerant bacteria with the capacity to reduce Se(IV) to Se(0) could benefit the DGR safety due to the immobilization of this metalloid, thus enhancing the repository's environmental safety.

CRediT authorship contribution statement

Marcos F. Martínez-Moreno: Writing – review & editing, Writing – original draft, Visualization, Validation, Project administration, Methodology, Investigation, Formal analysis, Data curation, Conceptualization. **Cristina Povedano-Priego:** Writing – review & editing, Validation, Methodology, Conceptualization. **Mar Morales-Hidalgo:** Writing – review & editing, Validation, Conceptualization. **Adam D. Mumford:** Writing – review & editing, Investigation, Formal analysis, Data curation. **Guillermo Lazuen-Lopez:** Writing – review & editing, Investigation. **Elisabet Aranda:** Writing – review & editing, Resources. **Ramiro Vilchez-Vargas:** Writing – review & editing, Resources, Formal analysis, Data curation. **Pier L. Solari:** Writing – review & editing, Resources, Formal analysis, Data curation. **Yon Ju-Nam:** Writing – review & editing, Supervision. **Fadwa Jroundi:** Writing – review & editing, Validation, Conceptualization. **Jesus J. Ojeda:** Writing – review & editing, Validation, Supervision, Resources, Investigation, Formal analysis, Conceptualization. **Mohamed L. Merroun:** Writing – review & editing, Visualization, Validation, Supervision, Resources, Project administration, Methodology, Funding acquisition, Conceptualization.

Funding

The present work was supported by the grant RTI2018-101548-B-

I00 “ERDF A way of making Europe” to MLM from the “Ministerio de Ciencia, Innovación y Universidades” (Spanish Government). The project leading to this application has received funding from the European Union's Horizon 2020 research and innovation programme under grant agreement No 847593 to MLM. ADM acknowledges funding from the UK Engineering and Physical Sciences Research Council (EPSRC) DTP scholarship (project reference: 2748843).

Declaration of competing interest

The authors declare that they have no known competing financial interests or personal relationships that could have appeared to influence the work reported in this paper.

Acknowledgements

The authors would like to thank Dr. F. Javier Huertas (IACT, Spain) for his invaluable guidance and assistance in the collection of bentonites from El Cortijo de Archidona. Rahul N. Doulatram Gamgaram and Maria del Carmen Contreras Morales (Institute of Water Research, University of Granada) for conducting the HPIC measurements. Daniel García-Muñoz Bautista-Cerro and Alicia González Segura (Centro de Instrumentación Científica, University of Granada, Spain) for their support with sample preparation and microscopy assistance, respectively.

Appendix A. Supplementary data

Supplementary data to this article can be found online at <https://doi.org/10.1016/j.scitotenv.2025.178613>.

Data availability

Data will be made available on request.

References

- Abdalla, Z.A.Y., Ismail, M.Y.A., Njoroge, E.G., Hlatshwayo, T.T., Wendler, E., Malherbe, J.B., 2020. Migration behaviour of selenium implanted into polycrystalline 3C-SiC. *Vacuum* 175, 109235. <https://doi.org/10.1016/j.vacuum.2020.109235>.
- Aoyagi, T., Mori, Y., Nanao, M., Matsuyama, Y., Sato, Y., Inaba, T., Hori, T., 2021. Effective Se reduction by lactate-stimulated indigenous microbial communities in excavated waste rocks. *J. Hazard. Mater.* 403, 123908. <https://doi.org/10.1016/j.jhazmat.2020.123908>.
- Avendaño, R., Chaves, N., Fuentes, P., Sánchez, E., Jiménez, J.I., Chavarría, M., 2016. Production of selenium nanoparticles in *Pseudomonas putida* KT2440. *Sci. Rep.* 6 (1), 37155. <https://doi.org/10.1038/srep37155>.
- Batandjéva, B., Delcheva, T., Duhovnik, B., 2009. Classification of Radioactive Waste: Safety Guide: IAEA General Safety Guide GSG-1. International Atomic Energy Agency, Vienna.
- Bengtsson, A., Pedersen, K., 2017. Microbial sulphide-producing activity in water saturated Wyoming MX-80, Asha and Calcigel bentonites at wet densities from 1500 to 2000 kg m⁻³. *Appl. Clay Sci.* 137, 203–212. <https://doi.org/10.1016/j.clay.2016.12.024>.
- Bienvenu, P., Cassette, P., Andreoletti, G., Bé, M.M., Comte, J., Lépy, M.C., 2007. A new determination of ⁷⁹Se half-life. *Appl. Radiat. Isot.* 65 (3), 355–364. <https://doi.org/10.1016/j.apradiso.2006.09.009>.
- Biesinger, M.C., 2017. Advanced analysis of copper X-ray photoelectron spectra. *Surf. Interface Anal.* 49 (13), 1325–1334. <https://doi.org/10.1002/sia.6239>.
- Breynaert, E., Scheinost, A.C., Dom, D., Rossberg, A., Vancluyse, J., Gobechiya, E., Kirschhock, C.E.A., Maes, A., 2010. Reduction of Se(IV) in boom clay: XAS solid phase speciation. *Environ. Sci. Technol.* 44, 6649–6655. <https://doi.org/10.1021/es100569e>.
- Chen, S., Wang, P., Zhang, D., 2014. Corrosion behavior of copper under biofilm of sulfate-reducing bacteria. *Corros. Sci.* 87, 407–415. <https://doi.org/10.1016/j.corsci.2014.07.001>.
- Dou, W., Pu, Y., Han, X., Song, Y., Chen, S., Gu, T., 2020. Corrosion of Cu by a sulfate reducing bacterium in anaerobic vials with different headspace volumes. *Bioelectrochemistry* 133, 107478. <https://doi.org/10.1016/j.bioelechem.2020.107478>.
- El-Batal, A.I., Mosallam, F.M., Ghorab, M.M., Hanora, A., Gobara, M., Baraka, A., El-Sayyad, G.S., 2020. Factorial design-optimized and gamma irradiation-assisted fabrication of selenium nanoparticles by chitosan and *Pleurotus ostreatus* fermented fenugreek for a vigorous in vitro effect against carcinoma cells. *Int. J. Biol. Macromol.* 156, 1584–1599. <https://doi.org/10.1016/j.ijbiomac.2019.11.210>.
- Eswayah, A.S., Smith, T.J., Scheinost, A.C., Hondow, N., Gardiner, P.H., 2017. Microbial transformations of selenite by methane-oxidizing bacteria. *Appl. Microbiol. Biotechnol.* 101, 6713–6724. <https://doi.org/10.1007/s00253-017-8380-8>.
- Fairley, N.CasaX.P.S., 2.3.22 ed.; Casa Software Ltd.: 2019.
- Freikowski, D., Winter, J., Gallert, C., 2010. Hydrogen formation by an arsenate-reducing *Pseudomonas putida*, isolated from arsenic-contaminated groundwater in West Bengal, India. *Appl. Microbiol. Biotechnol.* 88, 1363–1371. <https://doi.org/10.1007/s1201000988520>.
- García-Romero, E., Maríahuert Manchado, E., Suárez, M., García-Rivas, J., 2019. Spanish bentonites: a review and new data on their geology, mineralogy, and crystal chemistry. *Fortschr. Mineral.* 9, 696. <https://doi.org/10.3390/min9110696>.
- Gautam, A., Kushwaha, A., Rani, R., 2022. Reduction of hexavalent chromium [Cr(VI)] by heavy metal tolerant bacterium *Alkalihalobacillus clausii* CRA1 and its toxicity assessment through flow cytometry. *Curr. Microbiol.* 79 (1), 33. <https://doi.org/10.1007/s00284-021-02734-z>.
- Gebhardt, J.E., McCarron, J.J., Richardson, P.E., Buckley, A.N., 1986. The effect of cathodic treatment on the anodic polarization of copper sulfides. *Hydrometallurgy* 17 (1), 27–38. [https://doi.org/10.1016/0304-386X\(86\)90018-6](https://doi.org/10.1016/0304-386X(86)90018-6).
- Ghijsen, J., Tjeng, L.H., van Elp, J., Eskes, H., Westerink, J., Sawatzky, G.A., Czyzyk, M. T., 1988. Electronic structure of Cu₂O and CuO. *Phys. Rev. B* 38 (16), 11322–11330. <https://doi.org/10.1103/PhysRevB.38.11322>.
- Haghi, M., Diznabi, S.H., Karaboz, I., Omeroglu, E.E., 2023. Arsenic pollution and arsenic-resistant bacteria of drying Urmia Salt Lake. *Front. Environ. Sci.* 11, 1195643. <https://doi.org/10.3389/fenvs.2023.1195643>.
- Hall, D.S., Behazin, M., Binns, W.J., Keech, P.G., 2021. An evaluation of corrosion processes affecting copper-coated nuclear waste containers in a deep geological repository. *Prog. Mater. Sci.* 118, 100766. <https://doi.org/10.1016/j.pmatsci.2020.100766>.
- Hammer, O., Harper, D.A., 2001. PAST: Paleontological Statistics Software Package for Education and Data Analysis. *Palaeontol. Electron.* (<http://palaeo-electronica.org>).
- Hassan, R.S., Abass, M.R., Eid, M.A., Abdel-Galil, E.A., 2021. Sorption of some radionuclides from liquid waste solutions using anionic clay hydrotalcite sorbent. *Appl. Radiat. Isot.* 178, 109985. <https://doi.org/10.1016/j.apradiso.2021.109985>.
- He, R., Xia, F.F., Wang, J., Pan, C.L., Fang, C.R., 2011. Characterization of adsorption removal of hydrogen sulfide by waste biocover soil, an alternative landfill cover. *J. Hazard. Mater.* 186 (1), 773–778. <https://doi.org/10.1016/j.jhazmat.2010.11.062>.
- Hoving, A.L., Münch, M.A., Bruggeman, C., Banerjee, D., Behrends, T., 2019. Kinetics of selenite interactions with Boom Clay: adsorption–reduction interplay. *Geol. Soc., Lond. Spec. Publ.* 482, 225–239. <https://doi.org/10.1144/SP482-2018-60>.
- Huertas, F., Farina, P., Farias, J., García-Siñeriz, J.L., Villar, M.V., Fernández, A.M., Martín, P.L., Elorza, F.J., Gens, A., Sánchez, M., Lloret, A., Samper, J., Martínez, M.A., 2021. Full-scale Engineered Barriers Experiment. Updated Final Report, pp. 1994–2004.
- Johansson, A.J., Lilja, C., Sjögren, L., Gordon, A., Hallbeck, L., Johansson, L., 2017. Insights from post-test examination of three packages from the MiniCan test series of copper cast iron canisters for geological disposal of spent nuclear fuel: impact of the presence and density of bentonite clay. *Corros. Eng. Sci. Technol.* 52, 54–60. <https://doi.org/10.1080/1478422X.2017.1296224>.
- Jolley, J.G., Geesey, G.G., Hankins, M.R., Wright, R.B., Wichlacz, P.L., 1989. Auger electron and X-ray photoelectron spectroscopic study of the biocorrosion of copper by alginic acid polysaccharide. *Appl. Surf. Sci.* 37 (4), 469–480. [https://doi.org/10.1016/0169-4332\(89\)90505-9](https://doi.org/10.1016/0169-4332(89)90505-9).
- Jörg, G., Bühnenmann, R., Hollas, S., Kivel, N., Kossert, K., Van Winckel, S., Gostomski, C. L.V., 2010. Preparation of radiochemically pure ⁷⁹Se and highly precise determination of its half-life. *Appl. Radiat. Isot.* 68 (12), 2339–2351. <https://doi.org/10.1016/j.apradiso.2010.05.006>.
- Kang, M., Chen, F., Wu, S., Yang, Y., Bruggeman, C., Charlet, L., 2011. Effect of pH on aqueous Se(IV) reduction by pyrite. *Environ. Sci. Technol.* 45, 2704–2710. <https://doi.org/10.1021/es1033553>.
- Keech, P.G., Vo, P., Ramamurthy, S., Chen, J., Jacklin, R., Shoesmith, D.W., 2014. Design and development of copper coatings for long term storage of used nuclear fuel. *Corros. Eng. Sci. Technol.* 49 (6), 425–430. <https://doi.org/10.1179/1743278214Y.0000000206>.
- Le Caër, S., 2011. Water radiolysis: influence of oxide surfaces on H₂ production under ionizing radiation. *Water* 3 (1), 235–253. <https://doi.org/10.3390/w3010235>.
- Liu, D., Dong, H., Bishop, M.E., Zhang, J., Wang, H., Xie, S., Wang, S., Huang, L., Eberl, D.D., 2012. Microbial reduction of structural iron in interstratified illite-smectite minerals by a sulfate-reducing bacterium. *Geobiology* 10, 150–162. <https://doi.org/10.1111/j.1472-4669.2011.00307.x>.
- Mansour, A.N., 1994. Copper Mg Kα XPS spectra from the physical electronics model 5400 spectrometer. *Surf. Sci. Spectra* 3 (3), 202–210. <https://doi.org/10.1116/1.1247748>.
- Martínez-Moreno, M.F., Povedano-Priego, C., Morales-Hidalgo, M., Mumford, A.D., Ojeda, J.J., Jroundi, F., Merroun, M.L., 2023. Impact of compacted bentonite microbial community on the clay mineralogy and copper canister corrosion: a multidisciplinary approach in view of a safe Deep Geological Repository of nuclear wastes. *J. Hazard. Mater.* 131940. <https://doi.org/10.1016/j.jhazmat.2023.131940>.
- Martínez-Moreno, M.F., Povedano-Priego, C., Mumford, A.D., Morales-Hidalgo, M., Mijndendonckx, K., Jroundi, F., Ojeda, J.J., Merroun, M.L., 2024a. Microbial responses to elevated temperature: evaluating bentonite mineralogy and copper canister corrosion within the long-term stability of deep geological repositories of nuclear waste. *Sci. Total Environ.* 170149. <https://doi.org/10.1016/j.scitotenv.2024.170149>.

- Martinez-Moreno, M.F., Povedano-Priego, C., Morales-Hidalgo, M., Mumford, A.D., Aranda, E., Vilchez-Vargas, R., Merroun, M.L., 2024b. Microbial influence in Spanish bentonite slurry microcosms: unveiling a year long geochemical evolution and early-stage copper corrosion related to nuclear waste repositories. *Env. Poll.* 124491. <https://doi.org/10.1016/j.envpol.2024.124491>.
- Masurat, P., Eriksson, S., Pedersen, K., 2010. Microbial sulphide production in compacted Wyoming bentonite MX-80 under in situ conditions relevant to a repository for high-level radioactive waste. *Appl. Clay Sci.* 47, 58–64. <https://doi.org/10.1016/j.clay.2009.01.004>.
- Matschiavelli, N., Kluge, S., Podlech, C., Standhaft, D., Grathoff, G., Ikeda-Ohno, A., Cherkouk, A., 2019. The year-long development of microorganisms in uncompacted bavarian bentonite slurries at 30 and 60 °C. *Environ. Sci. Technol.* 53(10), 10514–10524. <https://doi.org/10.1021/acs.est.9b02670>.
- Meleshyn, A., 2011. Microbial processes relevant for long-term performance of radioactive waste repositories in clays. GRS-291. ISBN 978-3-939355-67-0. Available from: <https://www.grs.de/sites/default/files/pdf/GRS-291.pdf>.
- Miettinen, H., Bomberg, M., Bes, R., Tiljander, M., Vikman, M., 2022. Transformation of inherent microorganisms in Wyoming-type bentonite and their effects on structural iron. *Appl. Clay Sci.* 221, 106465. <https://doi.org/10.1016/j.clay.2022.106465>.
- Morales-Hidalgo, M., Povedano-Priego, C., Martinez-Moreno, M.F., Ruiz-Fresneda, M.A., Lopez-Fernandez, M., Jroundi, F., Merroun, M.L., 2024. Insights into the impact of physicochemical and microbiological parameters on the safety performance of Deep Geological Repositories. *Microorganisms* 12 (5), 1025. <https://doi.org/10.3390/microorganisms12051025>.
- Moulder, J.F., Stickle, W.F., Sobol, P.E., Bomben, K.D., 1992. *Handbook of X-Ray Photoelectron Spectroscopy*. Perkin-Elmer Corporation, Physical Electronics Division, Eden Prairie, Minn.
- Park, S.Y., Zhang, Y., O'Loughlin, E.J., Jo, H.Y., Kwon, J.S., Kwon, M.J., 2024. Temperature-dependent microbial reactions by indigenous microbes in bentonite under Fe (III)-and sulfate-reducing conditions. *J. Hazard. Mater.* 465, 133318. <https://doi.org/10.1016/j.jhazmat.2023.133318>.
- Patel, S., & Gupta, R. S. 2020. A phylogenomic and comparative genomic framework for resolving the polyphyly of the genus *Bacillus*: Proposal for six new genera of *Bacillus* species, *Peribacillus* gen. nov., *Cytobacillus* gen. nov., *Mesobacillus* gen. nov., *Neobacillus* gen. nov., *Metabacillus* gen. nov. and *Alkalihalobacillus* gen. nov. *Int. J. Syst. Evol. Microbiol.*, 70(1), 406–438. doi:<https://doi.org/10.1099/ijsem.0.003775>.
- Payer, J.H., Finsterle, S., Apps, J.A., Muller, R.A., 2019. Corrosion performance of engineered barrier system in deep horizontal drillholes. *Energies* 12, 1491. <https://doi.org/10.3390/en12081491>.
- Pentráková, L., Su, K., Pentrák, M., Stucki, J.W., 2013. A review of microbial redox interactions with structural Fe in clay minerals. *Clay Miner.* 48, 543–560. <https://doi.org/10.1180/claymin.2013.048.3.10>.
- Povedano-Priego, C., Jroundi, F., Lopez-Fernandez, M., Shrestha, R., Spanek, R., Martín-Sánchez, I., Villar, M.V., Sevcu, A., Dopson, M., Merroun, M.L., 2021. Deciphering indigenous bacteria in compacted bentonite through a novel and efficient DNA extraction method: insights into biogeochemical processes within the deep geological disposal of nuclear waste concept. *J. Hazard. Mater.* 408, 124600. <https://doi.org/10.1016/j.jhazmat.2020.124600>.
- Povedano-Priego, C., Jroundi, F., Solarí, P.L., Guerra-Tschuschke, I., del Mar Abad-Ortega, M., Link, A., Merroun, M.L., 2023. Unlocking the bentonite microbial diversity and its implications in selenium bioreduction and biotransformation: advances in Deep Geological Repositories. *J. Hazard. Mater.* 445, 130557. <https://doi.org/10.1016/j.jhazmat.2022.130557>.
- R Core Team, 2022. R: A Language and Environment for Statistical Computing. R Foundation for Statistical Computing, Vienna, Austria. <https://www.Rproject.org/>.
- Robertson, C.E., Harris, J.K., Wagner, B.D., Granger, D., Browne, K., Tatem, B., Feazel, L. M., Park, K., Pace, N.R., Frank, D.N., 2013. Explicit: graphical user interface software for metadata-driven management, analysis and visualization of microbiome data. *Bioinformatics* 29, 3100–3101. <https://doi.org/10.1093/bioinformatics/btt526>.
- Romand, M., Roubin, M., Deloume, J.P., 1978. ESCA studies of some copper and silver selenides. *J. Electron Spectros. Relat. Phenomena* 13 (3), 229–242. [https://doi.org/10.1016/0368-2048\(78\)85029-4](https://doi.org/10.1016/0368-2048(78)85029-4).
- Ruiz-Fresneda, M.A., Delgado-Martín, J., Gomez-Bolívar, J., Fernandez-Cantos, M.V., Bosch-Estévez, G., Martinez-Moreno, M.F., Merroun, M.L., 2018. Green synthesis and biotransformation of amorphous Se nanospheres to trigonal 1D se nanostructures: impact on Se mobility within the concept of radioactive waste disposal. *Environ. Sci. Nano* 5 (9), 2103–2116. <https://doi.org/10.1039/C8EN00221E>.
- Ruiz-Fresneda, M.A., Gomez-Bolivar, J., Delgado-Martin, J., Abad-Ortega, M.D.M., Guerra-Tschuschke, I., Merroun, M.L., 2019. The bioreduction of selenite under anaerobic and alkaline conditions analogous to those expected for a deep geological repository system. *Molecules* 24 (21), 3868. <https://doi.org/10.3390/molecules24213868>.
- Ruiz-Fresneda, M.A., Eswayah, A.S., Romero-González, M., Gardiner, P.H., Solarí, P.L., Merroun, M.L., 2020. Chemical and structural characterization of Se^{IV} biotransformations by *Stenotrophomonas bentonitica* into Se⁰ nanostructures and volatile Se species. *Environ. Sci. Nano* 7 (7), 2140–2155. <https://doi.org/10.1039/D0EN00507J>.
- Ruiz-Fresneda, M.A., Martinez-Moreno, M.F., Povedano-Priego, C., Morales-Hidalgo, M., Jroundi, F., Merroun, M.L., 2023. Impact of microbial processes on the safety of deep geological repositories for radioactive waste. *Front. Microbiol.* 14, 1134078. <https://doi.org/10.3389/fmicb.2023.1134078>.
- Ruiz-Fresneda, M.A., Staicu, L.C., Lazuén-López, G., Merroun, M.L., 2023b. Allotropy of selenium nanoparticles: Colourful transition, synthesis, and biotechnological applications. *J. Microbial. Biotechnol.* 16 (5), 877–892. <https://doi.org/10.1111/1751-7915.14209>.
- Salehi Alaei, E., Guo, M., Chen, J., Behazin, M., Bergendal, E., Lilja, C., Noël, J.J., 2023. The transition from used fuel container corrosion under oxic conditions to corrosion in an anoxic environment. *Mater. Corros.* 74 (11–12), 1690–1706. <https://doi.org/10.1002/maco.202313757>.
- Sanchez-Castro, I., Ruiz-Fresneda, M.A., Bakkali, M., Kämpfer, P., Glaeser, S.P., Busse, H. J., Merroun, M.L., 2017. *Stenotrophomonas bentonitica* sp. nov., isolated from bentonite formations. *Int. J. Syst. Evol. Microbiol.* 67 (8), 2779. <https://doi.org/10.1099/2fijsem.0.002016>.
- Shelobolina, E.S., VanPraagh, C.G., Lovley, D.R., 2003. Use of ferric and ferrous iron containing minerals for respiration by *Desulfitobacterium frappieri*. *Geomicrobiol. J.* 20, 143–156. <https://doi.org/10.1080/014904503003884>.
- Shiratori-Takano, H., Akita, K., Yamada, K., Itoh, T., Sugihara, T., Beppu, T., & Ueda, K. 2014. Description of *Symbiobacterium ostreiconchae* sp. nov., *Symbiobacterium turbinis* sp. nov. and *Symbiobacterium terracitae* sp. nov., isolated from shellfish, emended description of the genus *Symbiobacterium* and proposal of *Symbiobacteriaceae* fam. nov. *Int. J. Syst. Evol. Microbiol.*, 64(Pt 10), 3375–3383. doi:<https://doi.org/10.1099/ijse.0.063750-0>.
- Sitaud, B., Solarí, P.L., Schlut, S., Llorens, I., Hermange, H., 2012. Characterization of radioactive materials using the MARS beamline at the synchrotron SOLEIL. *J. Nucl. Mater.* 425 (1–3), 238–243. <https://doi.org/10.1016/j.jnucmat.2011.08.017>.
- Stackebrandt, E., Sproer, C., Rainey, F.A., Burghardt, J., Páuker, O., Hippe, H., 1997. Phylogenetic analysis of the genus *Desulfotomaculum*: evidence for the misclassification of *Desulfotomaculum guttoideum* and description of *Desulfotomaculum orientis* as *Desulfosporosinus orientis* gen. nov., comb. nov. *Int. J. Syst. Evol. Microbiol.* 47 (4), 1134–1139. <https://doi.org/10.1099/00207713-47-4-1134>.
- Staicu, L.C., Barton, L.L., 2021. Selenium respiration in anaerobic bacteria: does energy generation pay off? *J. Inorg. Biochem.* 222, 111509. <https://doi.org/10.1016/j.jinorgbio.2021.111509>.
- Staicu, L.C., Ackerson, C.J., Cornelis, P., Ye, L., Berendsen, R.L., Hunter, W.J., Pilon-Smits, E.A., 2015. *Pseudomonas moraviensis* subsp. stanleyae, a bacterial endophyte of hyperaccumulator *Stanleya pinnata*, is capable of efficient selenite reduction to elemental selenium under aerobic conditions. *J. Appl. Microbiol.* 119 (2), 400–410. <https://doi.org/10.1111/jam.12842>.
- Villar, M.V., Fernández-Soler, J.M., Delgado Huertas, A., Reyes, E., Linares, J., Jiménez de Cisneros, C., Linares, J., Reyes, E., Delgado, A., Fernandez-Soler, J.M., Astudillo, J., 2006. The study of Spanish clays for their use as sealing materials in nuclear waste repositories: 20 years of progress. *J. Iber. Geol.* 32, 15–36.
- Vogel, M., Fischer, S., Maffert, A., Hübner, R., Scheinost, A.C., Franzen, C., Steudtner, R., 2018. Biotransformation and detoxification of selenite by microbial biogenesis of selenium-sulfur nanoparticles. *J. Hazard. Mater.* 344, 749–757. <https://doi.org/10.1016/j.jhazmat.2017.10.034>.
- Wagner, C.D., Riggs, W.M., Davis, L.E., Moulder, J.F., Muilenberg, G.E., 1979. *Handbook of x-ray Photoelectron Spectroscopy: A Reference Book of Standard Data for Use in x-ray Photoelectron Spectroscopy*. Perkin-Elmer Corporation, Eden Prairie, MN.
- Wang, D., Rensing, C., Zheng, S., 2022. Microbial reduction and resistance to selenium: mechanisms, applications and prospects. *J. Hazard. Mater.* 421, 126684. <https://doi.org/10.1016/j.jhazmat.2021.126684>.
- Weser, U., Sokolowski, G., Pilz, W., 1977. Reaction of selenite with biochemically active thiols: an X-ray photoelectron spectroscopic study. *J. Electron Spectros. Relat. Phenomena* 10 (4), 429–439. [https://doi.org/10.1016/0368-2048\(77\)85039-1](https://doi.org/10.1016/0368-2048(77)85039-1).
- WNA, 2024. World Nuclear Association. Storage and disposal of radioactive waste. <https://www.world-nuclear.org/>.